

# Physical state of 21-cm absorber at $z_{\text{abs}} \sim 0.3$ towards a radio-loud quasar J1443+0214

IAS Summer Project Report

---

*ARIES, May 24, 2015 - July 20, 2015*

Avni Parmar  
M.Sc. Physics  
Savitribai Phule  
Pune University  
ap761144@gmail.com

Supervisor:  
Dr. Hum Chand  
Scientist D, ARIES  
humchand@gmail.com

# Contents

<b>Contents</b>	<b>i</b>
<b>List of Figures</b>	<b>iii</b>
<b>Acknowledgements</b>	<b>iv</b>
<b>1 Introduction to the project</b>	<b>1</b>
<b>2 Theoretical background and Literature survey</b>	<b>2</b>
2.1 Giant Meterwave Radio Telescope . . . . .	2
2.1.1 An Overview of GMRT . . . . .	2
2.1.2 Specifications of GMRT . . . . .	3
2.1.2.1 Antennas . . . . .	3
2.1.2.2 Observing Frequency Bands . . . . .	3
2.1.2.3 Bandwidth . . . . .	4
2.1.2.4 Resolution . . . . .	4
2.1.2.5 Field of View . . . . .	4
2.1.2.6 Radio Frequency Interference . . . . .	4
2.2 Synthesis Imaging in Radio Astronomy . . . . .	5
2.2.1 Coherence in Radio Astronomy . . . . .	5
2.2.1.1 Form of the Observed Electric field . . . . .	5
2.2.1.2 Spatial Coherence Function of the field . . . . .	7
2.2.2 Two Element Interferometer . . . . .	7
2.2.2.1 Response of an Interferometer . . . . .	7
2.2.2.2 The effect of bandwidth in two-element interferometer . . . . .	11
2.2.2.3 Delay tracking and frequency conversion . . . . .	12
2.2.2.4 Fringe rotation and Complex Correlators . . . . .	14
2.2.2.5 Coordinate systems for imaging . . . . .	15
2.2.2.6 Antenna spacings and $(u, v, w)$ components . . . . .	17
2.2.2.7 The effect of bandwidth in radio images . . . . .	20
2.2.3 The Primary Antenna Elements . . . . .	23
2.2.3.1 Introduction . . . . .	23
2.2.3.2 Basics of Antenna . . . . .	23
2.2.4 Editing and Calibration . . . . .	27
2.2.4.1 Editing/Flagging . . . . .	27
2.2.4.2 The need of flux calibrator and phase calibrators . . . . .	27
2.2.4.3 Gain Calibration . . . . .	28

---

2.2.4.4	Bandpass Calibration . . . . .	30
2.2.4.5	Deconvolution and Clean . . . . .	30
2.2.4.6	Self-Calibration . . . . .	34
2.3	Fundamentals of Radiative Transfer . . . . .	34
2.3.1	Specific Intensity . . . . .	34
2.3.2	Equation of Radiative Transfer . . . . .	35
2.3.3	Solution of the Radiative Transfer Equation and Optical Depth . . . . .	35
2.4	Neutral Hydrogen . . . . .	37
2.4.1	HI 21-cm Emission and Absorption . . . . .	37
2.4.2	Spin temperature . . . . .	37
<b>3</b>	<b>Data Analysis and Calculations</b>	<b>40</b>
3.1	Data Reduction using AIPS . . . . .	40
3.1.1	Glimpses of data reduction process in AIPS . . . . .	41
3.2	Gaussian fitting and Calculations using IDL . . . . .	45
<b>4</b>	<b>Results and Future work</b>	<b>47</b>
<b>5</b>	<b>References</b>	<b>48</b>
<b>A</b>	<b>Introduction to AIPS</b>	<b>49</b>
A.1	Introduction . . . . .	49
A.2	Tasks . . . . .	50
A.3	Verbs . . . . .	50
A.4	Adverbs . . . . .	50
A.5	AIPS message file . . . . .	51
A.6	Data files and Catalogues . . . . .	51
<b>B</b>	<b>Getting started with AIPS</b>	<b>56</b>
B.1	Starting the AIPS program . . . . .	56
<b>C</b>	<b>Step by Step manual for Absorption line Spectroscopy</b>	<b>58</b>
C.1	Loading the data . . . . .	58
C.2	Flagging and Editing . . . . .	60
C.3	Calibration . . . . .	62
C.3.1	Gain Calibration . . . . .	62
C.3.2	Bandpass Calibration . . . . .	66
C.3.3	Self Calibration . . . . .	69
C.4	Obtaining the spectrum . . . . .	71

# List of Figures

2.1	GMRT antennae configuration . . . . .	2
2.2	An astrophysical phenomenon . . . . .	6
2.3	Two element Interferometer . . . . .	8
2.4	Phase tracking center . . . . .	10
2.5	Schematic diagram of an interferometer with time delay . . . . .	12
2.6	RF, IF and LO relationship . . . . .	13
2.7	The $(u, v, w)$ and $(l, m, n)$ right-handed coordinate systems . . . . .	15
2.8	The trace of baseline vector $\mathbf{b}$ . . . . .	17
2.9	Coordinate system for specification of baseline parameters . . . . .	18
2.10	Relationship between $(X, Y, Z)$ and $(u, v, w)$ coordinate systems . . . . .	18
2.11	Projection of the baseline vector . . . . .	19
2.12	Effect of Bandwidth smearing . . . . .	21
2.13	Block diagram of the electronic equipment for correlation from one antenna pair . . . . .	24
2.14	The reception pattern of the antenna . . . . .	25
2.15	The Fourier transform relationship between an antenna aperture distribution and its far-field radiation pattern . . . . .	26
2.16	The GMRT UV coverage . . . . .	31
2.17	Geometry for ray-path integration for $I_\nu$ . . . . .	36
2.18	Hyperfine splitting of the 1s ground state of atomic Hydrogen . . . . .	38
3.1	AIPSTV screenshot of the Plot of Flux (Janskys) and Time (Hours) for source J1443+0214 . . . . .	41
3.2	Image of source J1443+0214 before self-calibration . . . . .	42
3.3	Step by step cleaning of image during self-calibration . . . . .	43
3.4	21-cm absorption line . . . . .	44
3.5	Gaussian fitting to the absorption line profile . . . . .	45
3.6	Optical depth of HI . . . . .	45



# Acknowledgements

*I take this opportunity to present this project on ‘Physical state of 21-cm absorber at  $z_{abs} \sim 0.3$  towards a radio-loud quasar J1443+0214 performed under the guidance of Dr. Hum Chand, Scientist D, ARIES.*

*I have no words to express my gratefulness towards my project guide who helped and supported me at each and every step for successful completion of the project. I am very glad and obliged that he gave me a new field of interest through this project and created a pathway for my future in Radio Astronomy. I thank him for greatly inspiring me and presenting me a new outlook towards learning fundamentals of Physics. So I express my deepest gratitude and respect to Hum Sir.*

*I would like to show my gratitude to Dr. S. I. Patil, Head of Physics Department, Savitribai Phule Pune University for recommending me for IAS Summer Research Fellowship and encouraging me.*

*A special thanks to Dr. Neeraj Gupta (IUCAA) and Dr. Amitesh Omar (ARIES) for their help and valuable comments which helped me to progress in my project work.*

*I wish to acknowledge the people at ARIES, specially Sumit Jaiswal (SRF), Alka Mishra (Post-Doc Fellow) and all my seniors - Parveen Kumar (SRF), Vidushi (JRF), Sapna (JRF) who have supported me in various ways throughout the project. I am equally thankful to people at Library and Computer section (ARIES), for their support.*

*I also thank my friends from Pune University - Vikram Jaiswal and Rajeev Singh for being with me at difficult times.*

*Finally, I take this chance to thank my parents and whole family for all their support and encouragement without which I wouldn't be able to give my best in this project.*

*I would not forget to thank and express gratitude to the Almighty and great Scientists for their precious gifts to the mankind. . . .*

# Chapter 1

## Introduction to the project

Understanding the physical state of the interstellar medium of protogalaxy at high redshift plays a key role in our understanding of galaxy formation. Although it is not possible to directly observe the highly redshifted galaxies, but their signature as absorption line in the background quasar spectrum allow us to study them in both optical and radio regions. In this regard we study the quasar-galaxy pair (QGP) J1443+0214 with  $z_{\text{qso}} = 1.82$ ,  $z_{\text{abs}} = 0.3714$ . The foreground galaxy in this QGP is identified by the detection of emission lines in the SDSS spectrum of QSO. The foreground galaxy is invisible otherwise.

The QGP J1443+0214 was observed on 2012 June 2 (5.7h on source) with Giant Meterwave Radio Telescope (GMRT) using a baseband bandwidth of 4.17 MHz split into 512 spectral channels centered on the redshifted 21-cm frequency of foreground galaxy.

We reduce the data using Astronomical Image Processing System (AIPS) to obtain HI 21-cm absorption line. This reduction process consists of steps like loading the data into AIPS, editing and flagging the bad data, calibrating it through various steps of gain calibration, bandpass calibration and finally the self calibration. Further, we fit Gaussian components to the continuum and absorption line profile separately; then divide the continuum from multi-channel source data using Interactive Data Language (IDL).

We estimate parameters like optical depth and spin temperature from this spectrum obtained.

## Chapter 2

# Theoretical background and Literature survey

### 2.1 Giant Meterwave Radio Telescope

#### 2.1.1 An Overview of GMRT

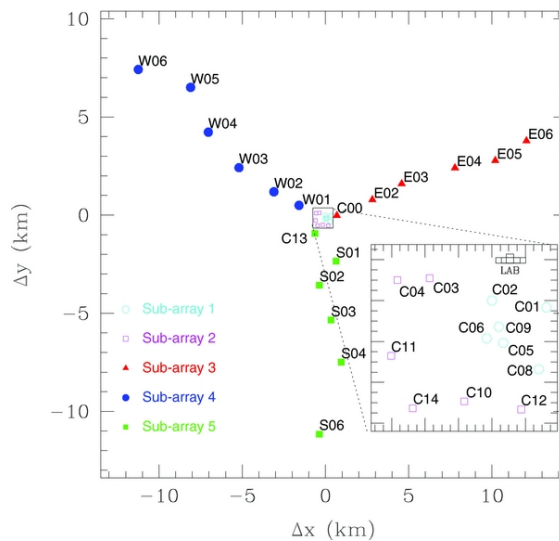


FIGURE 2.1: GMRT antennae configuration.

The Giant Meterwave Radio Telescope (GMRT) is located near Khodad village, which is about 80 km north of Pune. The GMRT consists of an array of 30 antennae, each of 45 m diameter, spread over a region of 25 km diameter. Amongst the multi-element earth rotation aperture synthesis telescopes operating at meter wavelengths, the GMRT has the largest collecting area. The interferometer has a hybrid configuration with 14 of its 30 antennas located in a central compact array with size  $\sim 1.1$  km and the remaining

antennas distributed in a roughly ‘Y’ shaped configuration, giving a maximum baseline length of  $\sim 25$  km. The baselines obtained from antennas in the are similar in length to the VLA D-array configuration, while the baselines between the arm antennas are comparable in length to the baseline lengths between VLA A-array and VLA B-array configurations. Hence, a single observation with the GMRT samples the  $(u, v)$  plane adequately on both short and long baselines with reasonable sensitivities. The GMRT can also be configured in array mode, where it acts as a single dish by adding the signals from individual dishes. This mode of operation is used for studying compact objects like pulsars, which are effectively point sources even for the largest interferometric baselines. The maximum instantaneous operating bandwidth at any frequency band is 33 MHz. Each antenna provides signals in two orthogonal polarisations, which are processed through a heterodyne receiver chain and brought to the central receiver building, where they are converted to baseband signals and fed to the digital back-end consisting of correlator and pulsar receiver.

## 2.1.2 Specifications of GMRT

### 2.1.2.1 Antennas

The GMRT antennas are alt-azimuth mounted parabolic prime-focus dishes. While the dishes can go down to an elevation of  $16^\circ$ , at present, the elevation limit has been set at  $17^\circ$ , giving a declination coverage from  $-53^\circ$  to  $+90^\circ$ . The slew speed of the antennas is  $20^\circ \text{ min}^{-1}$  on elevation axis and  $30^\circ \text{ min}^{-1}$  on azimuth axis, and they are not operated when winds are higher than  $40 \text{ km h}^{-1}$ . The reference antenna, C02 of the array is located at

latitude =  $19.1^\circ\text{N}$ ,

longitude =  $74.05^\circ\text{E}$ ,

altitude = 588 m.

### 2.1.2.2 Observing Frequency Bands

There is a rotating turret at the focus on which the different feeds are mounted. The feeds presently available are the 150, 325, 610/235 and the 1000 - 1450 MHz feeds. The 1000 - 1450 MHz feed, L-band feed is subdivided into 1060, 1170, 1280 and 1390 MHz sub-bands. The reflecting surface is formed by wire mesh and the efficiency of the antennas varies from 60% to 40%, from the lowest to the highest frequency. Both the orthogonal polarisations are brought to the control room from each antenna. The polarisations are circular for all feeds except the 1420 MHz feeds, which are linear. The 610 MHz and 235

MHz feeds are coaxial, allowing simultaneous dual frequency observations to be carried out at these two frequency bands, albeit for only one polarisation per band.

### 2.1.2.3 Bandwidth

The new GMRT Software Backend (GSB) supports a maximum bandwidth of 32 MHz. Users should consult the observatory regarding usable RF bandwidth at the lower frequencies because of RFI. For 150 MHz and 235 MHz, the recommended IF bandwidth is 6 MHz; however, 16 MHz is also usable, albeit with some caution.

### 2.1.2.4 Resolution

The approximate synthesized beam size (full width at half-maximum) for a full synthesis observation at each of the observing bands is given below:

150 MHz:  $\sim 20''$

235 MHz:  $\sim 13''$

325 MHz:  $\sim 9''$

610 MHz:  $\sim 5''$

1280 MHz:  $\sim 2''$

### 2.1.2.5 Field of View

The field of view, diffraction-limited response of the individual antennas is

$$\theta \simeq 85.2 \times \frac{325 \text{ GHz}}{\nu} \quad (2.1)$$

where  $\theta$ , the half-power beam-width is in arcmin and  $\nu$  is the frequency. These are

150 MHz:  $186' \pm 6'$

235 MHz:  $114' \pm 5'$

325 MHz:  $81' \pm 4'$

610 MHz:  $43' \pm 3'$

280 MHz:  $26.2' \pm 2'$

### 2.1.2.6 Radio Frequency Interference

Radio-frequency interference (RFI) signals are among the main factors limiting the performance of radio telescopes. RFI constricts the available frequency space, effectively increases system noise and corrupts calibration solutions. The effect is particularly

strong at frequencies below 1 GHz. Although, the RFI environment at GMRT is fairly decent, especially at frequencies below 235 MHz band it can be quite alarming. While the strongest source in a field is typically only a few Jy, the RFI can occasionally reach several hundred Jy in some channels in the 150 and 235 MHz bands. However broadband RFI of up to several tens of Jy causes even more damage: currently available tools, including the AIPS task FLGIT provide some solution.

As mentioned above, the RFI environment can be bad at 150 MHz and is sometimes a problem at 235 MHz; the situation is usually better at night time and on weekends. (For these two bands, it is recommended to use the solar attenuators in the common box, to minimize the possibilities of saturating the downstream electronic chain due to RFI.) Observations at 325 MHz can be hampered sometimes due to RFI from nearby aircraft activity, especially during day time. Due to increasing interference from mobile phone signals around 950 MHz, the all-pass mode at 1400 MHz band is no longer supported as an official mode, and consequently observations below 1000 MHz in this band are not supported. Even for the lowest of the 4 sub-bands of the 1400 MHz band (covering  $1060 \pm 60$  MHz), the user is advised to check for effects of RFI.

## 2.2 Synthesis Imaging in Radio Astronomy

### 2.2.1 Coherence in Radio Astronomy

#### 2.2.1.1 Form of the Observed Electric field

Consider that an astrophysical phenomenon occurs at location  $\mathbf{R}$ . This phenomenon causes a time-variable electric field which is denoted by  $\mathbf{E}(\mathbf{R}, t)$ . If we have a finite time interval of a varying field the magnitude of the field can be expressed as the real part of the sum of the Fourier series in which time-varying functions are simple exponentials. The coefficients of this series denoted as  $\mathbf{E}_\nu(\mathbf{R})$ , are called the *quasi-monochromatic components* of the electric field  $\mathbf{E}(\mathbf{R}, t)$ .

Consider only a single quasi-monochromatic component, realising that the total response is the sum of the responses to all the components. The linearity of the Maxwell's Equations allow us to superpose the fields produced at a test location by the various source points,

$$\mathbf{E}_\nu(\mathbf{r}) = \int \int \int P_\nu(\mathbf{R}, \mathbf{r}) \mathbf{E}_\nu(\mathbf{R}) dx dy dz. \quad (2.2)$$

The function  $P_\nu(\mathbf{R}, \mathbf{r})$  is called the *propagator*, and it describes how the electric field at  $\mathbf{R}$  influences the electric field at  $\mathbf{r}$ .

Now introducing some simplifying assumptions, first of which is to ignore the fact that

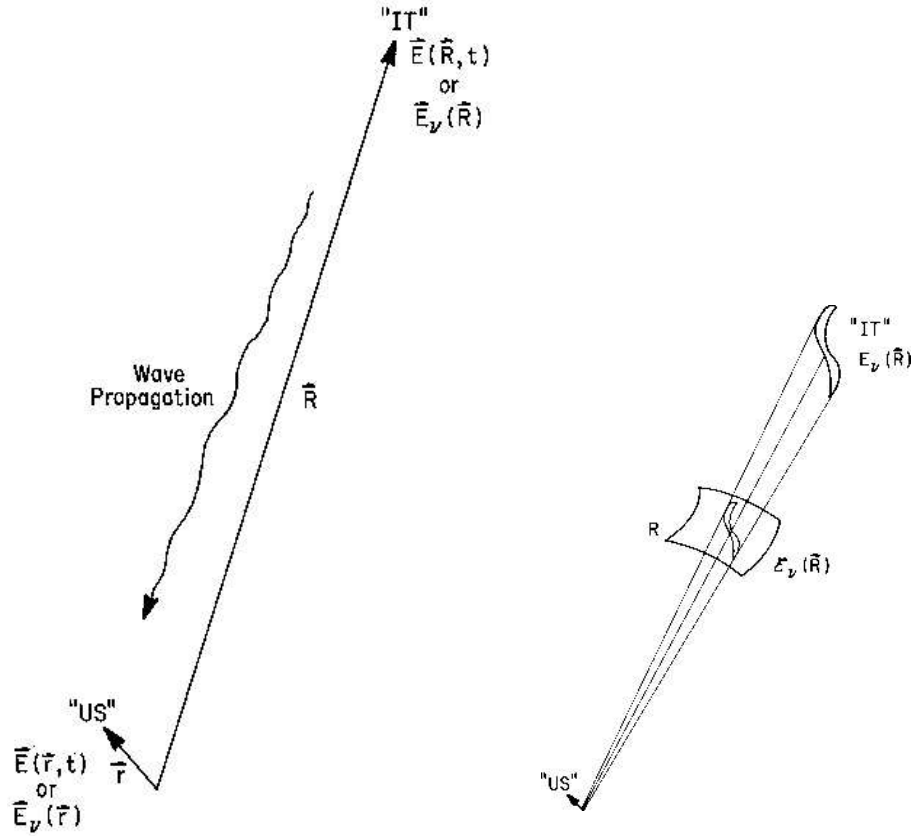


FIGURE 2.2: a.) An astrophysical phenomenon “IT”, located at  $\mathbf{R}$ , causes an electromagnetic wave  $\mathbf{E}_\nu(\mathbf{r})$  to propagate through space, where it can be detected at  $\mathbf{r}$  by “US”. b.) The passage of radiation from a distant source through an imaginary sphere at radius  $|\mathbf{R}|$  defines the electric distribution  $\epsilon_\nu(\mathbf{R})$  on this surface.

electromagnetic radiation is a vector phenomenon which enables the multiplication in Equation 2.2 to be regarded as ordinary scalar, and the *propagator*  $P$  to be an ordinary scalar function. The second assumption can be made by ignoring the structure of the emitting regions in third dimension i.e. in depth. Thus we replace the field strength  $E$  at the source with the field strength at convenient point, like one on the “celestial sphere” where the distribution of the source of fields can be considered as the distribution of the electric field on the surface of this sphere, which is denoted as  $\epsilon_\nu(\mathbf{R})$ .

The third simplifying assumption is that the space within the “celestial sphere” is empty. Then the Huygen’s Principle tells us that the propagator takes a particularly simple form as

$$E_\nu(\mathbf{r}) = \int \epsilon_\nu(\mathbf{R}) \frac{e^{2\pi i \nu |\mathbf{R}-\mathbf{r}|/c}}{|\mathbf{R}-\mathbf{r}|} dS, \quad (2.3)$$

where  $dS$  is the element of surface area of the celestial sphere.

### 2.2.1.2 Spatial Coherence Function of the field

The correlation of the field at the points  $\mathbf{r}_1$  and  $\mathbf{r}_2$  is defined as the expectation of the product ,

$$V_\nu(\mathbf{r}_1, \mathbf{r}_2) = \langle \mathbf{E}_\nu(\mathbf{r}_1) \mathbf{E}_\nu^*(\mathbf{r}_2) \rangle. \quad (2.4)$$

Substituting  $E_\nu(\mathbf{r})$ , from Equation 2.3,

$$V_\nu(\mathbf{r}_1, \mathbf{r}_2) = \left\langle \int \int \varepsilon_\nu(\mathbf{R}_1) \varepsilon_\nu^*(\mathbf{R}_2) \frac{e^{2\pi i \nu |\mathbf{R}_1 - \mathbf{r}_1|/c}}{|\mathbf{R}_1 - \mathbf{r}_1|} \frac{e^{2\pi i \nu |\mathbf{R}_2 - \mathbf{r}_2|/c}}{|\mathbf{R}_2 - \mathbf{r}_2|} dS_1 dS_2 \right\rangle. \quad (2.5)$$

The fourth simplifying assumption is that the radiation from astronomical objects is not spatially coherent, i.e.  $\langle \varepsilon_\nu(\mathbf{R}_1) \varepsilon_\nu^*(\mathbf{R}_2) \rangle$  is zero for  $\mathbf{R}_1 \neq \mathbf{R}_2$ . Exchanging the expectation and the integrals in Equation 2.5, we get

$$V_\nu(\mathbf{r}_1, \mathbf{r}_2) = \int \langle |\varepsilon_\nu(\mathbf{R})|^2 \rangle |\mathbf{R}|^2 \frac{e^{2\pi i \nu |\mathbf{R}_1 - \mathbf{r}_1|/c}}{|\mathbf{R}_1 - \mathbf{r}_1|} \frac{e^{2\pi i \nu |\mathbf{R}_2 - \mathbf{r}_2|/c}}{|\mathbf{R}_2 - \mathbf{r}_2|} dS. \quad (2.6)$$

Now writing  $\mathbf{s}$  for the unit vector  $\mathbf{R}/|\mathbf{R}|$  and  $I_\nu(\mathbf{s})$  for the observed intensity  $|\mathbf{R}|^2 \langle |\varepsilon_\nu(\mathbf{s})|^2 \rangle$ . Using the second assumption again to neglect the small terms of order  $|\mathbf{r}/\mathbf{R}|$ , and to replace the surface element  $dS$  on the celestial sphere by  $|\mathbf{R}|^2 d\Omega$ . Thus Equation 2.6 becomes

$$V_\nu(\mathbf{r}_1, \mathbf{r}_2) \approx \int I_\nu(\mathbf{s}) e^{-2\pi i \nu \mathbf{s} \cdot (\mathbf{r}_1 - \mathbf{r}_2)/c} d\Omega. \quad (2.7)$$

Equation 2.7 depends only on the separation vector  $\mathbf{r}_1 - \mathbf{r}_2$  of the two points, not on their absolute locations  $\mathbf{r}_1$  and  $\mathbf{r}_2$ . Therefore the correlation properties of the radiation field can be found by holding one observation point fixed and other moving around; thus we don't have to measure at all possible pairs of points. This function  $V_\nu$  of a single separation vector  $\mathbf{r}_1 - \mathbf{r}_2$  is called the spatial coherence function, of the field  $E_\nu(\mathbf{r})$ .

An interferometer is a device for measuring this spatial coherence function.

## 2.2.2 Two Element Interferometer

### 2.2.2.1 Response of an Interferometer

Synthesis arrays, which produce images by Fourier synthesis from measurement of complex visibility, can be analysed as ensembles of two-element interferometer. Consider an two-element interferometer in which the two antennas point toward a distant radio source in a direction indicated by a unit vector  $\mathbf{s}$ .  $\mathbf{b}$  is the interferometer baseline, and



the wavefront from the source reaches one antenna at a time  $\tau_g$  later than the other.  $\tau_g$  is the geometric delay and is given by,

$$\tau_g = \mathbf{b} \cdot \mathbf{s} / c \quad (2.8)$$

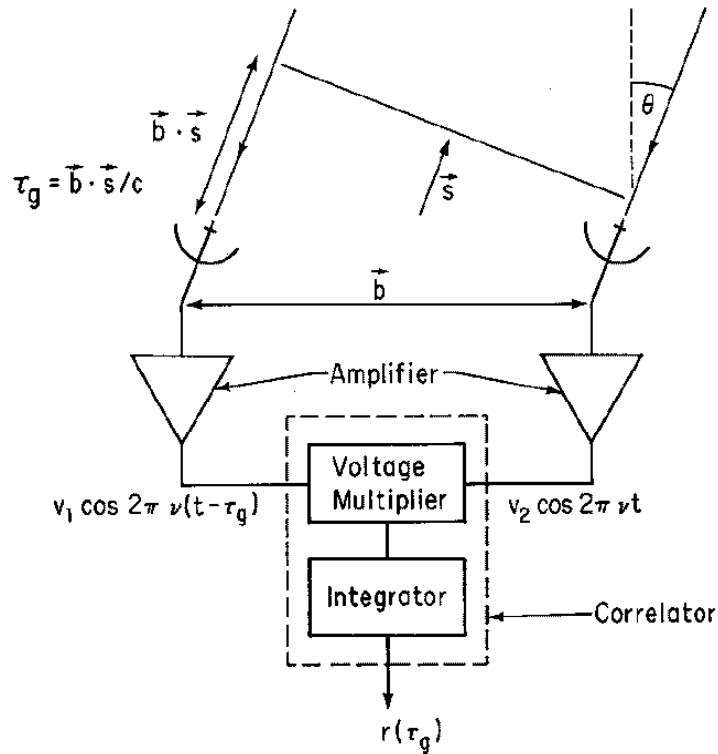


FIGURE 2.3: Schematic diagram of two-element interferometer

The signal from the antennas pass through amplifiers which incorporate filters to select the required frequency band of width  $\Delta\nu$  centered on frequency  $\nu$ . The components in which the the signals are combined ids the correlator; which is voltage multiplier followed by a time averaging circuit. If the input waveforms to the correlator are  $V_1(t)$  and  $V_2(t)$ , then the output is proportional to  $\langle V_1(t), V_2(t) \rangle$ . Representing the received signals by quasi-monochromatic Fourier components of frequency  $\nu$ ; which have the form  $V_1(t) = v_1 \cos 2\pi \nu (t - \tau_g)$ ,  $V_2(t) = v_2 \cos 2\pi \nu t$ .

The average output of the multiplier is

$$\begin{aligned}
 r(\tau_g) &= \int V_1(t)V_2(t).dt \\
 &= v_1v_2 \int [\cos 2\pi\nu(t - \tau_g).\cos 2\pi\nu t].dt, \\
 &= v_1v_2 \int [\cos^2(2\pi\nu t).\cos(2\pi\nu\tau_g) + \sin(2\pi\nu t).\sin(2\pi\nu\tau_g).\cos(2\pi\nu t)].dt, \\
 &= v_1v_2 \cos 2\pi\nu\tau_g,
 \end{aligned} \tag{2.9}$$

where we have assumed that the averaging time  $\Delta t \gg \frac{1}{\nu}$ .

$\tau_g$  varies slowly with time as the earth rotates, and the resulting oscillations of the cosine term represent the motion of the source through the interferometer fringe pattern. Now, express the interferometer output in terms of the radio brightness integrated over the sky. Let  $I(\mathbf{s})$  represent the radio brightness in the direction of unit vector  $\mathbf{s}$  at frequency  $\nu$ . Each antenna responds to a component of the input radiation field determined by the antenna polarization. The signal power received in bandwidth  $\Delta\nu$  from the source element  $d\Omega$  is  $A(\mathbf{s})I(\mathbf{s})\Delta\nu d\Omega$ , where  $A(\mathbf{s})$  is the effective collecting area in direction  $\mathbf{s}$ , which is to be same for each of the antennas. The resulting output from the correlator is proportional to the received power and to the cosine fringe term.

Therefore the output for the signal from solid angle  $d\Omega$  is

$$dr = A(\mathbf{s})I(\mathbf{s})\Delta\nu d\Omega \cos 2\pi\nu\tau_g. \tag{2.10}$$

In terms of the baseline and source position vectors,

$$r = \Delta\nu \int_S A(\mathbf{s})I(\mathbf{s})\cos\left(\frac{2\pi\nu\mathbf{b}\cdot\mathbf{s}}{c}\right) d\Omega, \tag{2.11}$$

where the integral is taken over the entire surface  $S$  of the celestial sphere, subtending  $4\pi$  steradians.

But in practice the integrand usually falls to very low values outside a small angular field as a result of the antenna bandwidth, the finite dimensions of the radio source, and other effects which restrict the field of view.

We have considered two assumptions in deriving the above Equation:

- i. The source field must be in the far field of the interferometer so that the incoming wavefronts can be considered to be plane.
- ii. The responses from different points in the source can be added independently. This requires that the source be spatially incoherent, i.e. the signal components emanating from different points on the source be uncorrelated.

When taking observation to make an interferometer image of a radio source, it is useful to specify a position on which the synthesized field of view is to be centered. This

position is referred to as the *phase tracking center* which can be represented by the vector  $\mathbf{s}_0$  as shown in Figure,  $\mathbf{s} = \mathbf{s}_0 + \sigma$ .

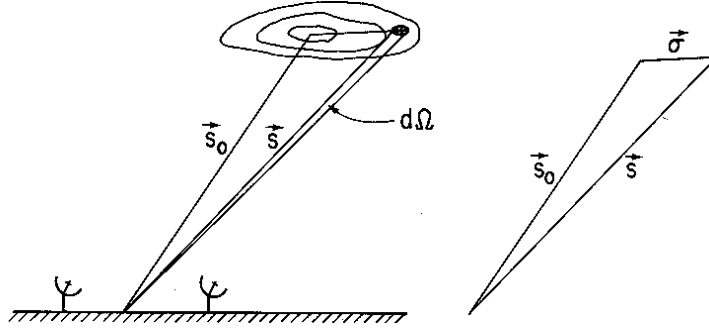


FIGURE 2.4: Position vectors used in deriving the response of the interferometer to the source which is represented by the contours of radio brightness  $I(\mathbf{s})$  on the sky.

From Equation 2.11 we obtain,

$$\begin{aligned}
 r &= \Delta\nu \int_S A(\mathbf{s})I(\mathbf{s})\cos 2\pi\nu\mathbf{b}\cdot\left(\frac{\mathbf{s}_0 + \sigma}{c}\right) d\Omega, \\
 &= \Delta\nu\cos\left(\frac{2\pi\nu\mathbf{b}\cdot\mathbf{s}_0}{c}\right) \int_S A(\sigma)I(\sigma)\cos\left(\frac{2\pi\nu\mathbf{b}\cdot\sigma}{c}\right) d\Omega, \\
 &\quad - \Delta\nu\sin\left(\frac{2\pi\nu\mathbf{b}\cdot\mathbf{s}_0}{c}\right) \int_S A(\sigma)I(\sigma)\sin\left(\frac{2\pi\nu\mathbf{b}\cdot\sigma}{c}\right) d\Omega.
 \end{aligned} \tag{2.12}$$

In radio astronomy, visibility is a complex quantity, the magnitude of which has the dimensions of spectral power flux density ( $Wm^{-2}Hz^{-1}$ ). It can be regarded as the unnormalized measure of the coherence of the electric field, modified to some extent by the characteristics of the interferometer.

The complex visibility of the source is defined as

$$V \equiv |V| e^{i\phi_v} = \int_S \mathcal{A}(\sigma)I(\sigma)e^{\frac{-2\pi i\nu\mathbf{b}\cdot\sigma}{c}} d\Omega, \tag{2.13}$$

where  $\mathcal{A}(\sigma) \equiv A(\sigma)/A_0$  is the normalized antenna reception pattern,  $A_0$  being the response at the beam center. We are considering the case in which the antennas track the source, and the system therefore responds to the modified brightness distribution  $\mathcal{A}(\sigma)I(\sigma)$ . By separating the real and imaginary parts of  $V$  in Equation 2.13 we obtain

$$A_0 |V| \cos\phi_v = \int_S A(\sigma)I(\sigma)\cos\left(\frac{2\pi\nu\mathbf{b}\cdot\sigma}{c}\right) d\Omega, \tag{2.14}$$

and

$$A_0 |V| \sin\phi_v = - \int_S A(\sigma) I(\sigma) \sin\left(\frac{2\pi\nu\mathbf{b}\cdot\sigma}{c}\right) d\Omega. \quad (2.15)$$

Substituting Equations 2.14 and 2.15 in Equation 2.12 gives

$$r = A_0 \Delta\nu |V| \cos\left(\frac{2\pi\nu\mathbf{b}\cdot\mathbf{s}_0}{c} - \phi_v\right). \quad (2.16)$$

The brightness distribution function of the source is obtained from the visibility data by inversion of the transformation in the Equation 2.13. Thus  $V$  must be measured over a sufficiently wide range of  $\nu\mathbf{b}\cdot\sigma/c$ , which is the component of the baseline normal to the direction of the source and measured in wavelengths.

### 2.2.2.2 The effect of bandwidth in two-element interferometer

Since the frequency of the cosine fringe term in Equation 2.16 is proportional to the observing frequency  $\nu$ , observing with a finite bandwidth  $\Delta\nu$  results, in effect, in the combination of fringe patterns with a corresponding range of fringe frequencies. With an infinitesimal bandwidth  $d\nu$ , the response can be written as

$$dr = A_0 |V| \cos(2\pi\nu\tau_g - \phi_v) d\nu. \quad (2.17)$$

Then for a rectangular frequency passband, the interferometer response is

$$\begin{aligned} r &= A_0 |V| \int_{\nu_0 - \Delta\nu/2}^{\nu_0 + \Delta\nu/2} \cos(2\pi\nu\tau_g - \phi_v) d\nu, \\ &= A_0 |V| \left[ \frac{\sin(2\pi\nu\tau_g - \phi_v)}{2\pi\tau_g} \right]_{\nu_0 - \Delta\nu/2}^{\nu_0 + \Delta\nu/2}, \\ &= \left[ \frac{A_0 |V|}{2\pi\tau_g} \right] [\sin(2\pi\nu_0\tau_g - \phi_v + \pi\Delta\nu\tau_g) - \sin(2\pi\nu_0\tau_g - \phi_v - \pi\Delta\nu\tau_g)], \quad (2.18) \\ &= \left[ \frac{A_0 |V|}{2\pi\tau_g} \right] [2\cos(2\pi\nu_0\tau_g - \phi_v) \sin(\pi\Delta\nu\tau_g)], \\ &= A_0 |V| \Delta\nu \frac{\sin\pi\Delta\nu\tau_g}{\pi\Delta\nu\tau_g} \cos(2\pi\nu_0\tau_g - \phi_v), \end{aligned}$$

where  $\nu_0$  is the center frequency of the observing passband. Thus in the system that we considering the fringes are modulated by a *sinc* function envelope, also referred to as

the *bandwidth pattern*. The full fringe amplitude is observed only when the source is in a direction normal to the baseline so that  $\tau_g = 0$ .

### 2.2.2.3 Delay tracking and frequency conversion

A block diagram of an interferometer system that includes an instrumental compensating delay is shown in the Figure 2.5 Frequency conversion of the incoming signals at radio frequency  $\nu_{RF}$  with a local oscillator at frequency  $\nu_{LO}$  is also included. Practical receiving systems incorporate frequency conversion because it is technically more convenient to perform functions such as amplification, filtering, delaying, and cross-correlating of the signals at an intermediate frequency that is lower than  $\nu_{RF}$  and remains fixed when the observing frequency is changed. The signals at the frequencies  $\nu_{RF}$  and  $\nu_{LO}$  are combined in a mixer which contains a non-linear element in which combinations of two frequencies are formed. The intermediate frequency  $\nu_{IF}$  is related to the mixer input frequencies by

$$\nu_{RF} = \nu_{LO} \pm \nu_{IF}. \quad (2.19)$$

$\nu_{LO}$  is a single-valued frequency, but  $\nu_{RF}$  and  $\nu_{IF}$  refer to bands of width  $\Delta\nu$ . Thus the mixer responds to inputs in two frequency bands, as shown in Figure 2.6 these are referred to as the upper lower sidebands and correspond to the + and - signs in Equation 2.19 respectively.

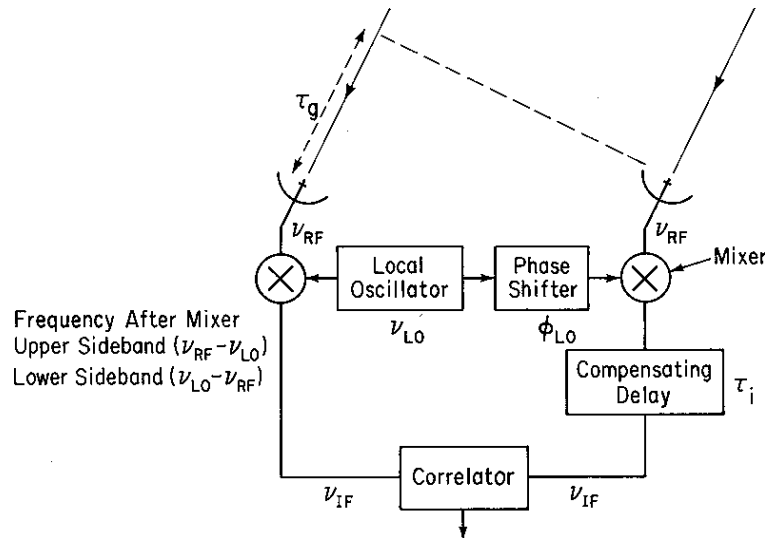


FIGURE 2.5: Schematic diagram of an interferometer incorporating frequency conversion and time delay to compensate for  $\tau_g$ .

For observations at frequencies up to a few tens of gigahertz the signal from each antenna

is usually first applied to a low-noise amplifier to obtain high sensitivity, and then passed through a filter that transmits only one of the two sidebands to the mixer. the response of such a single-sideband system can be obtained by considering the phase changes  $\phi_1$  and  $\phi_2$  imposed upon the signals received by antennas 1 and 2 before reaching the correlator inputs.

For the upper sideband case we have

$$\begin{aligned}\phi_1 &= 2\pi\nu_{RF}\tau_g = 2\pi(\nu_{LO} + \nu_{IF})\tau_g, \\ \phi_2 &= 2\pi\nu_{IF}\tau_i + \phi_{LO},\end{aligned}\tag{2.20}$$

where

$\phi_{LO} \rightarrow$  difference in the phase of the local oscillator signal at the two mixers.

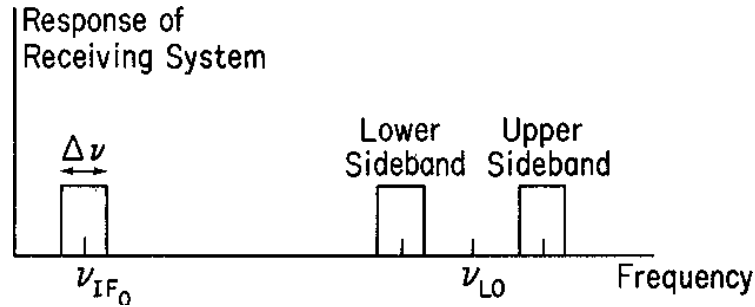


FIGURE 2.6: Relationship of RF, IF and LO frequencies

The upper sideband response of the interferometer is obtained by replacing the argument of the cosine function in Equation 2.17 by  $\phi_1 - \phi_2 - \phi_v$ ,  $d\nu$  by  $d\nu_{IF}$ ,

$$\begin{aligned}dr &= A_0 |V| \cos(\phi_1 - \phi_2 - \phi_v) d\nu_{IF}, \\ &= A_0 |V| \cos[2\pi(\nu_{LO}\tau_g + \nu_{IF}\tau_g - \nu_{IF}\tau_i) - \phi_v - \phi_{LO}], \\ &= A_0 |V| \cos[2\pi(\nu_{LO}\tau_g + \nu_{IF}\Delta\tau) - \phi_v - \phi_{LO}],\end{aligned}\tag{2.21}$$

where  $\Delta\tau = \tau_g - \tau_i$  is the tracking error of the compensating delay  $\tau_i$ .

Now, integrating with respect to  $\nu_{IF}$  from  $\nu_{IF_0} - \Delta\nu/2$  to  $\nu_{IF_0} + \Delta\nu/2$  we get,

$$r_u = A_0 \Delta\nu |V| \frac{\sin\pi\Delta\nu\Delta\tau}{\pi\Delta\nu\Delta\tau} \cos[2\pi(\nu_{LO}\tau_g + \nu_{IF}\Delta\tau) - \phi_v - \phi_{LO}].\tag{2.22}$$

The output fringe oscillations, which result from the time variation of  $\tau_g$ , in this case depend upon the local oscillator frequency  $\nu_{LO}$  rather than that of the observing frequency at the antenna as in Equation 2.16

Similarly the response in case of lower sideband is

$$r_l = A_0 \Delta \nu |V| \frac{\sin \pi \Delta \nu \Delta \tau}{\pi \Delta \nu \Delta \tau} \cos[2\pi(\nu_{LO} \tau_g - \nu_{IF} \Delta \tau) - \phi_v - \phi_{LO}]. \quad (2.23)$$

#### 2.2.2.4 Fringe rotation and Complex Correlators

The output from the correlator represented by Equations 2.22, 2.23 is fed to a computer which performs some form of optimal analysis to determine the amplitude and phase of the fringe oscillations. The fringe visibility  $V$  can then be obtained by calibration of the instrumental parameters. This calibration usually involves observation of one or more sources with known positions, flux densities, and angular dimensions. To preserve the fringe information it is necessary to sample the correlator output at least twice per fringe period. Thus the data rate to the computer can be very much higher than that necessary to follow the changes in the visibility  $V$ , for which values at intervals of order one second are likely to be adequate. However, by inserting progressively varying phase shifts in the local oscillator signals it is possible to slow down the fringe oscillations, and reduce the computation required. Thus in Equations 2.22, 2.23 if we vary  $\phi_{LO}$  so that  $(2\pi\nu_{LO}\tau_g - \phi_{LO})$  remains constant, the correlator output will vary only as a result of changes in  $V$  and slow drifts in the instrumental parameters. This procedure, in which  $\phi_{LO}$  is usually controlled by the same computer that regulates the delay tracking, is referred to as *fringe rotation* or *fringe stopping*. The effect of compensating delay  $\tau_i$  tracking  $\tau_g$  is to cause the envelope the fringe pattern to follow the source across the sky, and to change the frequency of the fringes by a factor  $\nu_{LO}/\nu_0$  for a single-sideband receiving system. If  $\tau_i$  were inserted at the received signal frequency, the fringe frequency would be reduced to zero without the adjustment of the local oscillator phase.

After fringe stopping, the output of the correlator in Figure 2.5 is a slowly varying voltage (a constant voltage for the case of a point source at the phase tracking center). To measure the complex fringe amplitude in this case a scheme using two correlators, as shown in Figure 2.6 can be used. For each antenna pair a second correlator with a  $\pi/2$  phase shift in one input is added. the response of the second correlator can be obtained by replacing  $\phi_1$  in Equation 2.20 by  $\phi_1 - \pi/2$ . Then in Equations 2.22, 2.23 the cosine term containing  $\tau_g$  becomes a sine, with no change in the argument. Such a scheme is usually referred to as a *complex correlator*. In addition to allowing the visibility to be measured with zero frequency, the complex correlator provides an improvement of  $\sqrt{2}$  in signal-to-noise ratio over a single correlator, since the noise fluctuations at the two outputs are uncorrelated.

## 2.2.2.5 Coordinate systems for imaging

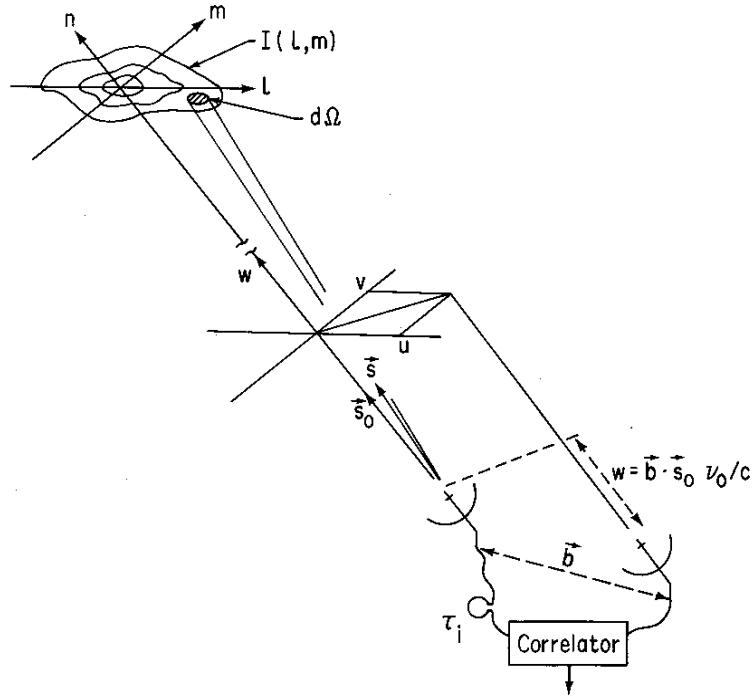


FIGURE 2.7: The  $(u, v, w)$  and  $(l, m, n)$  right-handed coordinate systems used to express the interferometer baselines and the source brightness distribution, respectively.

The baseline vector has components  $(u, v, w)$  where  $w$  points in the direction of interest, i.e. towards a position  $\mathbf{s}_0$  that becomes the center of the synthesized image. The components  $u$ ,  $v$ , and  $w$  are measured in wavelengths at the center frequency of the RF signal band, and in directions towards the East, the North and the phase tracking center, respectively. Positions in the sky are defined in  $l$  and  $m$ , which are the direction cosines measured with respect to the  $u$  and  $v$  axes. A synthesized image in the  $(l, m)$  plane represents a projection of the celestial sphere onto a tangent plane at the  $(l, m)$  origin. Distances in  $l$  and  $m$  are proportional to the sines of the angles measured from the origin, which is a convenient practical system. In these coordinates the parameters used in the derivation of the interferometer response in terms of visibility in Equations becomes,

$$\frac{\nu \mathbf{b} \cdot \mathbf{s}}{c} = ul + vm + wn, \quad \text{and} \quad \frac{\nu \mathbf{b} \cdot \mathbf{s}_0}{c} = w, \quad (2.24)$$

$$d\Omega = \frac{dl \, dm}{n} = \frac{dl \, dm}{\sqrt{1 - l^2 - m^2}}.$$



Thus in the coordinates of Figure 2.7,

$$\frac{\nu \mathbf{b} \cdot \boldsymbol{\sigma}}{c} = \frac{\nu \mathbf{b} \cdot (\mathbf{s} - \mathbf{s}_0)}{c}, \quad (2.25)$$

in Equation 2.13 becomes

$$V(u, v, w) = \int_{-\infty}^{\infty} \int_{-\infty}^{\infty} \mathcal{A}(l, m) I(l, m) e^{-2\pi i [ul + vm + w(n-1)]} \frac{dl \, dm}{\sqrt{1 - l^2 - m^2}}, \quad (2.26)$$

$$V(u, v, w) = \int_{-\infty}^{\infty} \int_{-\infty}^{\infty} \mathcal{A}(l, m) I(l, m) e^{-2\pi i [ul + vm + w(\sqrt{1-l^2-m^2}-1)]} \frac{dl \, dm}{\sqrt{1 - l^2 - m^2}},$$

where the integrand is taken to be zero for  $l^2 + m^2 \geq 1$ . The complex visibility is expressed as a function of  $(u, v, w)$ , since these are the coordinates that represent the spacings of the antennas with respect to the phase tracking center of the source,  $\mathbf{s}_0$ . The visibility is also a function of the modified brightness distribution  $\mathcal{A}I$ .

It is desirable to reduce Equation 2.26 to the form of a two-dimensional Fourier transform so as to simplify its inversion, by means of which  $I(l, m)$  is obtained from the visibility. This can be done under two sets of conditions. The first when the baselines are coplanar, which can be understood by considering the way in which the Earth's rotation carries the antenna through space. It is evident from the Figure 2.8 that the rotation causes the tip of the baseline vector to trace out a circle concentric with the Earth's rotation axis.

The rising and setting of a point on the sky usually limit the range over which  $V$  can be measured to an arc of the circle. In general, for a two-dimensional array of antennas on the surface of the Earth, the circular loci resulting from the different baselines have different diameters and lie in different planes. However, for the particular case of an array of antennas in an East-West line on the Earth's surface, the components of the baseline vector parallel to the Earth's axis are zero, and the baseline-vectors are coplanar.

Then, if we choose the  $w$  - axis to lie in the direction of the celestial pole, so that  $w = 0$ , Equation 2.26 becomes

$$V(u, v, w) = \int_{-\infty}^{\infty} \int_{-\infty}^{\infty} \mathcal{A}(l, m) I(l, m) e^{-2\pi i (ul + vm)} \frac{dl \, dm}{\sqrt{1 - l^2 - m^2}}, \quad (2.27)$$

The inverse of above two-dimensional Fourier transform is

$$\frac{\mathcal{A}(l, m) I(l, m)}{\sqrt{1 - l^2 - m^2}} = \int_{-\infty}^{\infty} \int_{-\infty}^{\infty} V(u, v) e^{2\pi i (ul + vm)} du \, dv. \quad (2.28)$$

When for a two-dimensional array of antennas the baseline vectors do not remain coplanar in  $(u, v, w)$  space a system of three coordinates is required to accommodate the

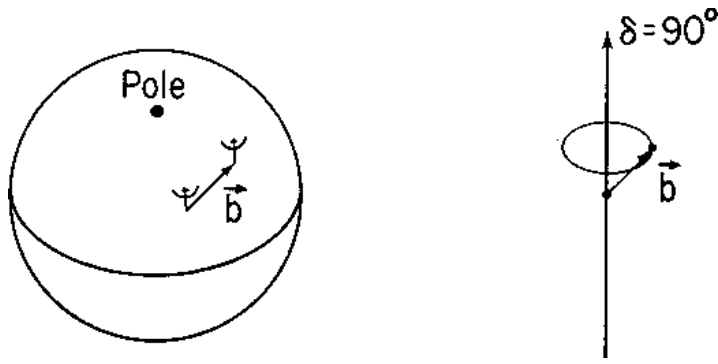


FIGURE 2.8: The baseline vector  $\mathbf{b}$  traces out a circular locus in a plane normal to the direction of declination ( $\delta$ ) equal to  $90^\circ$ , as the Earth rotates.

spacing vectors. Now we consider the second set of conditions under which the Equation 2.26 reduces to a two-dimensional Fourier transform. These depend on  $|l|$  and  $|m|$  being small enough that we can write

$$(\sqrt{1 - l^2 - m^2} - 1)w \approx -\frac{1}{2}(l^2 + m^2)w \approx 0. \quad (2.29)$$

Then Equation 2.26 becomes

$$V(u, v, w) = \int_{-\infty}^{\infty} \int_{-\infty}^{\infty} \mathcal{A}(l, m) I(l, m) e^{-2\pi i(ul+vm)} dl dm. \quad (2.30)$$

For  $|l|$  and  $|m|$  small, i.e. small field imaging, the dependence of the visibility upon  $w$  is very small and can be omitted. From Equation 2.30 we can write

$$\mathcal{A}(l, m) I(l, m) = \int_{-\infty}^{\infty} \int_{-\infty}^{\infty} V(u, v) e^{2\pi i(ul+vm)} du dv. \quad (2.31)$$

### 2.2.2.6 Antenna spacings and $(u, v, w)$ components

With multiple-element antenna arrays, it is convenient to specify the antenna positions relative to some reference point measured in a cartesian coordinate system. For example, a system with axes pointing towards hour-angle  $h$  and declination  $\delta$  equal to  $(h = 0, \delta = 0)$  for  $X$ ,  $(h = -6^h, \delta = 0)$  and  $(\delta = 90^\circ)$  for  $Z$  may be used as shown in the Figure 2.9.

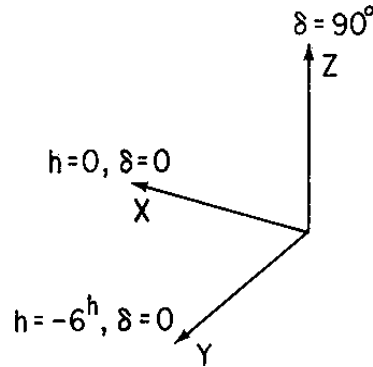


FIGURE 2.9: Coordinate system for specification of baseline parameters. X is the direction of the meridian at the celestial equator, Y is toward the East and Z toward the North celestial pole.

Then if  $L_X, L_Y$  and  $L_Z$  are the corresponding coordinate differences for two antennas, the baseline components  $(u, v, w)$  are given by,

$$\begin{pmatrix} u \\ v \\ w \end{pmatrix} = \frac{1}{\lambda} \begin{pmatrix} \sin H_0 & \cos H_0 & 0 \\ -\sin \delta_0 \cos H_0 & \sin \delta_0 \sin H_0 & \cos \delta_0 \\ \cos \delta_0 \cos H_0 & -\cos \delta_0 \sin H_0 & \sin \delta_0 \end{pmatrix} \begin{pmatrix} L_X \\ L_Y \\ L_Z \end{pmatrix}$$

where  $H_0$  and  $\delta_0$  are the hour-angle and the declination of the phase reference position, and  $\lambda$  is the wavelength corresponding to the center frequency of the receiving system. The elements in the transformation matrix are the direction cosines of the  $(u, v, w)$  axes relative to  $(X, Y, Z)$  axes as shown in Figure 2.10.

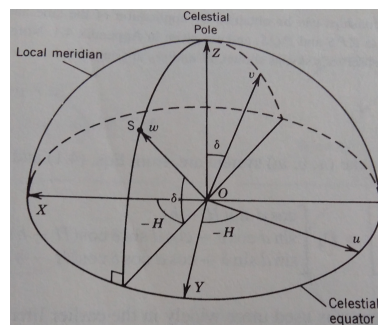


FIGURE 2.10: Relationship between  $(X, Y, Z)$  and  $(u, v, w)$  coordinate systems. The  $(u, v, w)$  system is defined for observation in the direction of point  $S$  which has hour angle  $H$  and declination  $\delta$ . The direction cosines in the transformation matrix below follow from the relationships in this diagram.

By eliminating  $H_0$  from the expressions for  $u$  and  $v$  we obtain the equation of an ellipse

in the  $(u, v)$  plane.

$$u^2 + \left( \frac{v - (L_Z/\lambda)\cos\delta_0}{\sin\delta_0} \right)^2 = \frac{L_X^2 + L_Y^2}{\lambda^2}. \quad (2.32)$$

Thus as the interferometer observes a point on the celestial sphere, the rotation of the Earth causes the  $u$  and  $v$  components of the baseline to trace out an elliptical locus. This ellipse is simply the projection onto the  $(u, v)$  plane of the circular locus traced out by the tip of the baseline vector as shown earlier in the Figure 2.8. Since  $I(l, m)$  is real,  $V(-u, -v) = V^*(u, v)$ , and at any instant the correlator output provides the measure of the visibility at two points in the  $(u, v)$  plane as shown in the Figure 2.11.

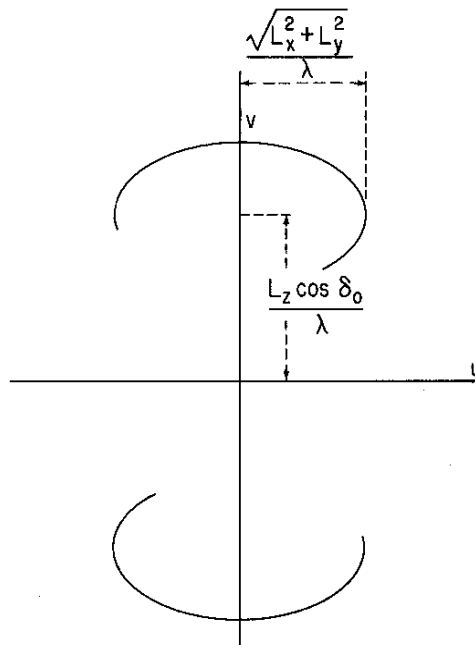


FIGURE 2.11: Elliptical loci representing the projection of the baseline vector onto the  $(u, v)$  plane as a source is tracked across the sky.

For an array of antennas the ensemble of elliptical loci is known as the *transfer function* or *sampling function*,  $S(u, v)$ , which is the function of the declination of the observation as well as of the antenna spacings. The transfer function indicates the values of  $u$  and  $v$  at which the visibility function is sampled. Since the visibility function for a point source at the  $(l, m)$  origin is a constant in  $u$  and  $v$ , the Fourier transform of the transfer function indicates the response to a point source, i.e. the synthesized beam. In designing arrays the principal aim is to obtain transfer functions that cover the  $(u, v)$  plane as widely as uniformly as possible. An interferometer responds to structure on the

sky with spatial frequency  $u$  cycles per radian in the  $l$ -direction and  $v$  cycles per radian in the  $m$ -direction. The transfer function of an array therefore indicates its response as a spatial frequency filter.

### 2.2.2.7 The effect of bandwidth in radio images

As seen in section 2.2.2.2, the effect of a finite receiving bandwidth  $\Delta\nu$  is to modulate the fringes with an envelope function of width inversely proportional to  $\Delta\nu$ , and that as a result we must insert an instrumental delay  $\tau_i$  to compensate the geometrical delay  $\tau_g$ . This compensation is exact only for the radiation from the center of the synthesized field, which is usually chosen as the delay tracking center. Variation of  $\tau_g$  causes radial blurring of the image.

So far we have considered that all our measurements are made at one particular radio frequency (RF), defined as channel zero previously. But, in practice the instrument has a finite bandwidth around the frequency of interest, as shown in the Figure 2.12. All the quantities that were introduced previously are in principle functions of frequency as well. As for example,

$V_{ij}(u, v) \rightarrow V_{ij}(u, v, \nu)$ ,  $\mathcal{A}(l, m) \rightarrow \mathcal{A}(l, m, \nu)$ ,  $G_{ij}(t) \rightarrow G_{ij}(t, \nu)$ , and so forth.

In observing continuum radiation one is interested in the mean brightness over the bandwidth  $\Delta\nu$ , and the visibility data are processed as though they were all observed at the center frequency  $\nu_0$  as shown in Figure 2.12.

Thus, we need to integrate over the frequency dependent part as well. As shown in section 2.2.2.2, we consider the integral over the bandwidth, for the spatial coherence function  $r$ ,

$$r = A_0 |V| \Delta\nu \frac{\sin\pi\Delta\nu\tau_g}{\pi\Delta\nu\tau_g} \cos(2\pi\nu_0\tau_g - \phi_v). \quad (2.33)$$

Thus, from the Equation it is clear that the visibility would get modulated by a *sinc* function if there is finite bandwidth. This is called *fringe washing*.

In particular, the spatial frequency coordinates in the  $(u, v)$  plane are calculated for the band center. Let these be  $(u_0, v_0)$  for frequency  $\nu_0$  and  $(u_\nu, v_\nu)$  for another frequency  $\nu$  within the receiving band. Since  $u_\nu$  and  $v_\nu$  represent projected antenna spacings measured in wavelengths, we can write

$$u_0 = \frac{X}{\lambda_0} = \frac{X}{\lambda_\nu} \frac{\lambda_\nu}{\lambda_0} \equiv u_\nu \frac{\nu_0}{\nu} \quad \text{and} \quad v_0 = \frac{Y}{\lambda_0} = \frac{Y}{\lambda_\nu} \frac{\lambda_\nu}{\lambda_0} \equiv v_\nu \frac{\nu_0}{\nu} \quad (2.34)$$

This implies,

$$(u_0, v_0) = \left( \frac{\nu_0}{\nu} u_\nu, \frac{\nu_0}{\nu} v_\nu \right). \quad (2.35)$$

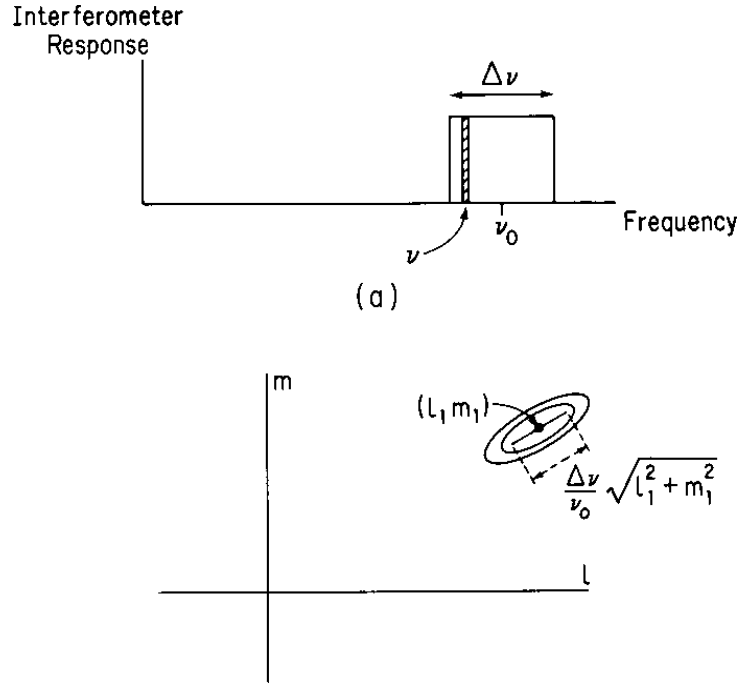


FIGURE 2.12: Idealized rectangular response showing center frequency  $\nu_0$  and a narrow band with bandwidth  $\Delta\nu$  (above). The radial smearing of a point source at  $(l_1, m_1)$  in the synthesized image (below).

Now, consider the visibility that corresponds to a very small band of frequencies centered on  $\nu$  as in Figure 2.12. This band contributes a component of brightness  $I$  to the synthesized image which is related to the corresponding visibility by,

$$V(u, v) \rightleftharpoons I(l, m),$$

where the symbol  $\rightleftharpoons$  indicates that the two functions constitute a Fourier transform pair, and here we have omitted the functions  $\mathcal{A}(l, m)$  and  $\frac{1}{\sqrt{1-l^2-m^2}}$  which are usually close to unity. The processes of correlation and Fourier transformation are linear, and that they allow us to consider the synthesized image as the sum of the series of contributions from different parts of the frequency passband. In the derivation of the radio image we assign values  $u_0$  and  $v_0$  to  $V$  which are the true values multiplied by  $(\frac{\nu_0}{\nu})$  as in Equation 2.35. The effect in the image can be obtained from the similarity theorem of Fourier transforms for n-dimensions which is

$$\mathcal{FT}[f(ax)] = \frac{1}{|a|^n} F\left(\frac{u}{a}\right), \quad \text{where} \quad F(u) = \mathcal{FT}[f(x)]. \quad (2.36)$$

Thus,

$$V(u_0, v_0) = V\left(\frac{\nu_0}{\nu} u_\nu, \frac{\nu_0}{\nu} v_\nu\right) \rightleftharpoons \left(\frac{\nu}{\nu_0}\right)^2 I\left(\frac{\nu}{\nu_0} l, \frac{\nu}{\nu_0} m\right). \quad (2.37)$$

This implies that the co-ordinates of the brightness function  $I$  gets scaled by a factor of  $\left(\frac{\nu}{\nu_0}\right)$ , and a factor  $\left(\frac{\nu}{\nu_0}\right)^2$  appears in the amplitude to conserve the total integrated brightness. Thus, for the upper end of the bandwidth, i.e. frequency  $\nu_0 + \Delta\nu/2$ , a point source at  $(l_1, m_1)$ , will be scaled and will be shown at a coordinate,  $\left(\frac{\nu_0 + \Delta\nu/2}{\nu_0} l_1, \frac{\nu_0 + \Delta\nu/2}{\nu_0} m_1\right)$ . Similarly, for the lower end of the bandwidth,  $\nu_0 - \Delta\nu/2$ , the co-ordinate would be shifted at,  $\left(\frac{\nu_0 - \Delta\nu/2}{\nu_0} l_1, \frac{\nu_0 - \Delta\nu/2}{\nu_0} m_1\right)$ . So, as shown in Figure 2.11, a point source at  $(l_1, m_1)$  would get smeared into a line of length,

$$d = \sqrt{\left(\frac{\nu_0 + \Delta\nu/2 - \nu_0 + \Delta\nu/2}{\nu_0}\right)^2 l_1^2 + \left(\frac{\nu_0 + \Delta\nu/2 - \nu_0 + \Delta\nu/2}{\nu_0}\right)^2 m_1^2} \quad (2.38)$$

$$= \left(\frac{\nu}{\nu_0}\right) \sqrt{(l_1^2 + m_1^2)}$$

along the radial direction. This is called as *bandwidth smearing*. Thus the angular extent of the smearing at a radial distance  $\sqrt{(l^2 + m^2)}$  from the origin is approximately equal to  $\left(\frac{\nu}{\nu_0}\right) \sqrt{(l^2 + m^2)}$ , and the effect becomes important at distances for which the smearing is comparable with the synthesized beamwidth. An alternative method of imaging with a wide bandwidth is by using a multi-channel receiving system, in which the passband is divided into  $n$  frequency channels of width  $\Delta\nu/n$ . Separate correlators are used for each frequency channel, so the visibility values for each one can be associated with the values of  $u$  and  $v$  corresponding to the center frequency of the channel. Such systems are also used for spectral line observations. In the  $(u, v)$  plane the elliptical track that represents the projected spacing for any pair of antennas is replaced by a series of  $n$  parallel tracks. In effect the overall transfer function is the sum of  $n$  single channel functions, each scaled in  $u$  and  $v$  in proportion to the corresponding center frequency of the receiving channel. The sum of the corresponding images shows no radial smearing, but since the angular scale of the synthesized beam (point spread function) varies from channel to the next, the effect of averaging the beam profiles is to reduce the unwanted sidelobes.

For example:

The FX correlator used in GMRT splits the entire bandwidth of 16 MHz (for a typical continuum observation) into 128 narrower frequency bands of 125 KHz each, called channels. This feature helps us to reduce the effect of bandwidth smearing, by averaging for smaller channel widths, the imaging algorithm effectively sees this truncated bandwidth. Clearly, the effect of bandwidth smearing can be neglected if the smeared length is of the order of the highest resolution, i.e, the synthesised beam,  $\theta_{synth} = \lambda/d$ , where  $d$  is the size of the entire array or the maximum baseline (for GMRT,  $d \sim 25km$ ). If one wants to image the entire primary beam then  $max | \sqrt{l^2 + m^2} |, \forall(u, v)$ , corresponds

to half the size of the primary beam,  $\theta_{pri} = \lambda/D$ . Here,  $D$  is the size of the antenna (for GMRT,  $D = 45m$ ). Thus the required bandwidth,  $\Delta\nu^{reqd}$ , to avoid appreciable bandwidth smearing,

$$\frac{\Delta\nu^{reqd}}{\nu_0} \sqrt{l^2 + m^2} \sim \theta_{synth}, \quad i.e. \quad \frac{\Delta\nu^{reqd}}{\nu_0} \frac{\theta_{pri}}{2} \sim \theta_{synth}. \quad (2.39)$$

Therefore, we have the condition,

$$\frac{\Delta\nu^{reqd}}{\nu_0} \sim \frac{2\theta_{synth}}{\theta_{pri}}. \quad (2.40)$$

## 2.2.3 The Primary Antenna Elements

### 2.2.3.1 Introduction

The important properties of the primary antenna that can affect the image include aperture efficiency, pointing accuracy, beam circularity, sidelobe level, polarization purity and noise temperature. Figure 2.13 shows the simple block diagram of the major pieces of equipment required in a synthesis telescope.

The primary antenna can be defined as the piece of equipment that intercepts the propagating electromagnetic wave from the observed source and makes a sample of it available at the input to the first low-noise amplifier, either as an electric current on a cable or as a field in a single mode waveguide. Thus for reflector antennas the feed and its polarization splitter can be included as the part of antenna. At the output of the antenna the signal is at the radio, or sky frequency  $\nu_{RF}$ . The signal undergoes various frequency translations as it propagates through the electronic system as shown in the Figure 2.13.

### 2.2.3.2 Basics of Antenna

Now we discuss standard antenna formulas useful in understanding how the properties of the primary antenna element affect a synthesized image. Consider the effective collecting area of the primary antenna  $A(\nu, \theta, \phi)$  (in units of  $m^2$ ), where  $\nu$  is the frequency and  $\theta$ ,  $\phi$  are the direction coordinates. If the antenna is pointed to a source with brightness  $I(\nu, \theta, \phi) Wm^{-2}Hz^{-1}sr^{-1}$ , as in Figure 2.14 then the power  $P$  (in Watts) received by the antenna in bandwidth  $\Delta\nu$  from element  $\Delta\Omega$  of solid angle is given by

$$P = A(\nu, \theta, \phi)I(\nu, \theta, \phi)\Delta\nu\Delta\Omega. \quad (2.41)$$



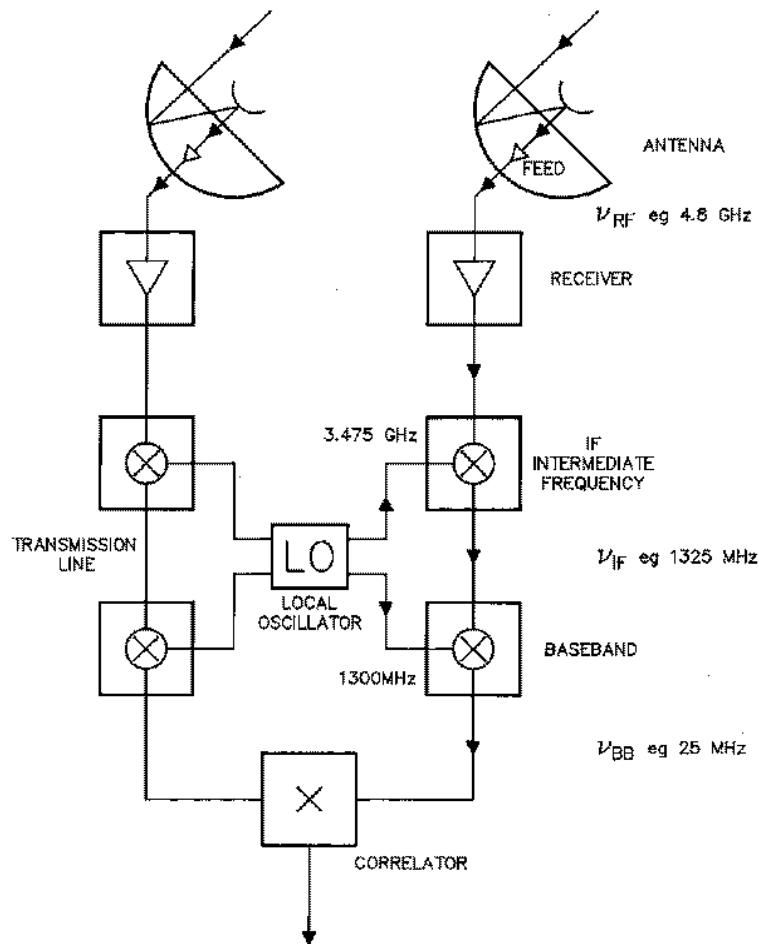


FIGURE 2.13: A simplified block diagram of the electronic equipment used to produce the correlation from one antenna pair in a synthesis telescope.

The normalized antenna reception pattern  $\mathcal{A}$ , or the power pattern is defined as

$$\mathcal{A}(\nu, \theta, \phi) = A(\nu, \theta, \phi)/A_0, \quad (2.42)$$

where  $A_0(m^2)$  is the response at the center of the main lobe of  $A(\nu, \theta, \phi)$  and is called the effective area of the antenna.

The beam solid angle,  $\Omega_A$ , of the power pattern is defined as

$$\Omega_A = \int \int_{all\ sky} \mathcal{A}(\theta, \phi) d\Omega. \quad (2.43)$$

An important fundamental relationship in antenna theory states that the product of the effective area and the beam solid angle is equal to the square of the wavelength,

$$A_0 \Omega_A = \lambda^2. \quad (2.44)$$

$\Omega_A$  is the measure of the field of view of the synthesis telescope. If  $\mathcal{A}$  is everywhere equal to 1, then  $\Omega_A$  has its maximum possible value of  $4\pi$  and the primary antenna is isotropic and can see the whole sky with equal sensitivity.

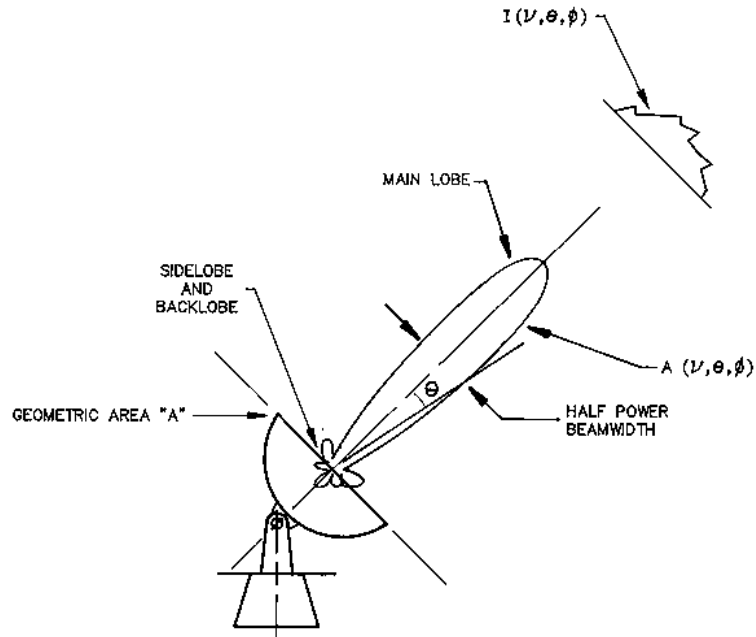


FIGURE 2.14: The reception pattern of the antenna.

For antennas that have a well defined physical collecting area, the ratio of  $A_0$  to the physical area  $A$  of the aperture is called the *aperture efficiency*  $\eta$ , a dimensional quantity less than unity,

$$A_0 = \eta A. \quad (2.45)$$

The final antenna relationship is the Fourier transform relationship between the complex voltage distribution of the field,  $f(u, v)$ , in the aperture of the antenna and the complex far-field voltage radiation pattern,  $F(l, m)$ , of the antenna,

$$F(l, m) = \int \int_{\text{aperture}} f(u, v) e^{2\pi i(ul+vm)} du dv, \quad (2.46)$$

and

$$f(u, v) = \int_{-\infty}^{\infty} \int_{-\infty}^{\infty} F(l, m) e^{2\pi i(ul+vm)} dl dm. \quad (2.47)$$

The form of  $f(u, v)$  and  $F(l, m)$  is shown in the Figure 2.15,

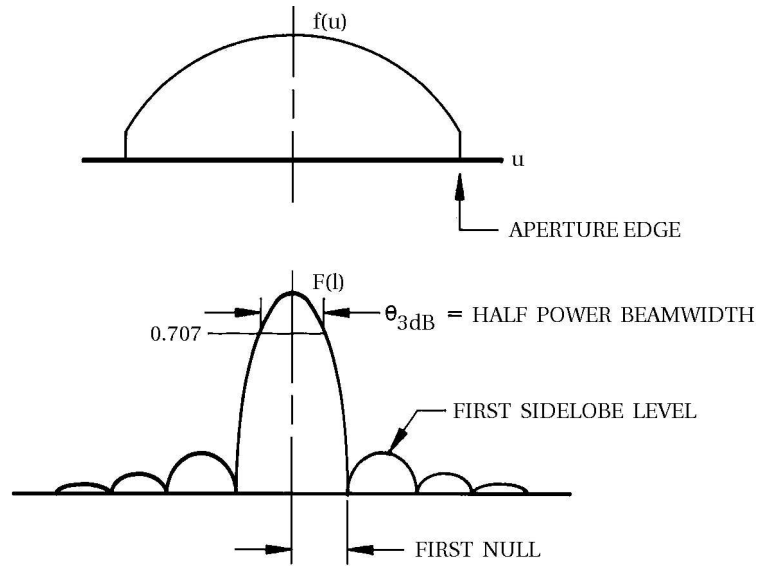


FIGURE 2.15: The Fourier transform relationship between an antenna aperture distribution and its far-field radiation pattern.

The radiation pattern coordinates are given by

$$u = \sin\theta \cos\phi \quad \text{and} \quad v = \sin\theta \sin\phi. \quad (2.48)$$

The voltage and the power patterns are related by  $\mathcal{A} = |F|^2$ . The Fourier transform relationship between an antenna aperture distribution and its radiation pattern is analogous to the one between the source brightness distribution and its visibility function. Both antenna radiation pattern and source visibility function have the same general form of a main central lobe surrounded by lesser sidelobes, but the radiation pattern does not have to be Hermitian (i.e. need not be conjugate symmetric).

The form of  $f(u, v)$  for an antenna is determined by the way in which the antenna feed illuminates the aperture. In general, the more that  $f(u, v)$  is tapered at the edge of the aperture, the lower will be the aperture efficiency and the sidelobes, the broader will be the main beam.

## 2.2.4 Editing and Calibration

### 2.2.4.1 Editing/Flagging

When parts of an array malfunction, data of poor quality are recorded, and their inclusion in the imaging process will deteriorate the results. Even if it is possible to calibrate the severely affected data, it may have too much noise or may be unstable. Data of poor quality are usually worse than no data at all. It is impossible to display all of data from modern synthesis telescopes. By carefully choosing a subset of representative data, it is usually possible to discover faulty data in nearly all of the data set, and edit it.

Editing of array data is usually done in the four steps:

1. Determining which antennas are working.
2. Removing outliers and looking for inconsistent data.
3. This part of editing is done during the calibration process, when longer-term problems come to light and more subtle problems may surface.
4. The last step comes after the image is made. If this image is of poor quality, then more data editing may be required or the calibration may be in error.

### 2.2.4.2 The need of flux calibrator and phase calibrators

A strong calibrator source is observed to determine various instrumental parameters. This source is commonly referred to as the primary calibrator or the flux calibrator. The primary calibrator is a strong point source which is observed generally at the beginning and end of the observation. Thus, all the baselines see similar flux except multiplied with a gain factor. In practice the gain and the phase of a interferometer changes over a timescale of a few minutes due to various instrumental and atmospheric reasons. The ionosphere continuously changes and thereby causes irregularities in the phase of the wavefronts. Since, the aperture synthesis telescopes like GMRT, are very large, different antennas sees through different patch of ionosphere. There are large scale, slowly varying refractive index gradient in the ionosphere which can make source position to wander. This puts a constrain on the distance of the calibrators with respect to the source. To study these phase and amplitude changes to a reasonable accuracy, the calibrator should not be very far from the target source, else we would be correcting for an entirely different patch of the ionosphere which may not be applicable to the target source. Also these calibrator sources should themselves not vary with time. But the reality is such that there are very few sources whose fluxes remain unchanged. Therefore, the

possibility to find calibrator near to the target source ( $\sim 5 - 20$  degrees) is very rare. This necessitates the use of another calibrator called secondary calibrator or the phase calibrator. The flux calibrator observed at the beginning and end of an observation run is used to calibrate for the fluxes of the phase calibrator. Typically the fluxes of a flux calibrator remain unchanged for a few tens of years, while for the phase calibrator the fluxes changes in order of days, but remains stable during a typical observation run.

### 2.2.4.3 Gain Calibration

The equation for the sky brightness distribution, i.e.  $I_\nu(l, m)$  from Equation 2.31, can be rewritten as

$$I_\nu(l, m) = \int \int \mathcal{A}_\nu(l, m) V_\nu(u, v) e^{2\pi i(ul+vm)} du dv. \quad (2.49)$$

Equation 2.49 says that the sky brightness distribution is just a Fourier transform of the visibility given by Equation 2.31. That means to determine,  $I_\nu(l, m)$ , we need to know all the Fourier components,  $V_\nu(u, v)$ , i.e. continuous determination of visibility at all possible  $(u, v)$ . But, in practice we have finite number of antennas placed discretely, which means, that the visibilities are sampled at discrete times for each pair of antennas. Therefore, Equation 2.49 can be written as,

$$V_{ij}(t) = \int_{-\infty}^{\infty} \int_{-\infty}^{\infty} \mathcal{A}_\nu(l, m) I_\nu(l, m) e^{-2\pi i[u_{ij}(t)l+v_{ij}(t)m]} dl dm. \quad (2.50)$$

Aperture synthesis essentially consists of measuring the Fourier components of the source brightness distribution as much as possible. Each baseline precisely measures these Fourier components at each instant of time. The inverse Fourier transform of which gives us  $I_\nu(l, m)$ . A pair of antenna essentially measures the complex visibilities multiplied with the gain of the receiver and an additive system noise. Good engineering assures that the aperture synthesis arrays are, to a good approximation, linear devices. Also, measurements made by one pair of antenna are independent of measurements by any other two pair. This allows us to write

$$V_{ij}^{obs}(t) = G_{ij} V_{ij}(t) + \epsilon_{ij}(t) + \eta_{ij}(t). \quad (2.51)$$

where,

$t \rightarrow$  time of the observation,

$V_{ij}^{obs}(t) \rightarrow$  the observed visibility,

$V(t) \rightarrow$  the true visibility,

$G(t) \rightarrow$  the baseline based complex gain,

$\epsilon_{ij}(t) \rightarrow$  the baseline based complex offset and  
 $\eta_{ij}(t) \rightarrow$  the random noise.

These extra complex factors are a measure of both amplitude and phase errors introduced by the interferometer. These errors are also due the distortion of the wave planes, caused by the intervening medium between the source and the observer. To measure the correct visibility at a given time for a particular baseline, we need to solve for the  $G_{ij}$ s and the phase associated. Equation 2.51 can be modified to determine the baseline based gains. For a given pair of antenna,  $i$  and  $j$ , we consider that the baseline based offsets,  $\epsilon_{ij}(t)$  and  $\eta_{ij}(t)$  be included in baseline based complex gain factor. That is, we consider the additive terms as combined within the complex gain and redefine the gain as,

$$G_{ij}(t) = G_{ij}^{ante}(t) + \epsilon'_{ij}(t) + \eta'_{ij}(t). \quad (2.52)$$

Here,  $G_{ante}(t)$  is baseline based gain without the effect of any offset. The prime on  $\epsilon$  and  $\eta$  indicates that they are not the same as defined in Equation 2.51. It can be written as,  $G_{ante}(t) = g_i(t)g_j^*(t)$ , where,  $g_i(t)$ s are the antenna based complex gains. Now, by combining the two offset terms as,  $\kappa_{ij}(t) = \epsilon_{ij}(t) + \eta_{ij}(t)$ , we can write,

$$G_{ij}(t) = g_i(t)g_j^*(t) + \kappa_{ij}(t). \quad (2.53)$$

We now consider that additive offset term is negligible as compared to the antenna based gain terms. If this approximation is not true then these would manifest in the form of calibration errors and are required to be flagged. Now, we neglect this additive term and write the gain as,  $G_{ij}(t) = g_i(t)g_j^*(t)$ . Therefore, from Equation 2.51, we get,

$$V_{ij}^{obs}(t) = G_{ij}(t)V_{ij}(t). \quad (2.54)$$

The process of calibration is used to determine the complex antenna based gain,  $g_i(t)$ s. If there are  $N$  antennas, then observations of calibrators determine the  ${}^N C_2 = N(N - 1)/2, G_{ij}$ s. Other properties helps to determine the  $N$  number of antenna based gains. We have seen that the gain,  $G_{ij}(t)$ , can be written as antenna based terms only,

$$\begin{aligned} G_{ij}(t) &= g_i(t)g_j^*(t) = a_i(t)e^{i\phi_i(t)}(a_j(t)e^{i\phi_j(t)})^*, \\ &= a_i(t)a_j(t)e^{i(\phi_i(t)-\phi_j(t))}, \\ &= G_{ij}^{ante}(t)e^{i(\phi_i(t)-\phi_j(t))}. \end{aligned} \quad (2.55)$$

where,  $a_{i,j}(t)$  are the antenna based amplitude corrections and  $\phi_{i,j}(t)$  are the antenna based phase corrections. We define an antenna based amplitude gain,  $G_{ij}^{ante}(t) =$

$a_i(t)a_j(t)$ . Thus, from Equations 2.50 and 2.54 we get, using Equation 2.55:

$$V_{ij}^{obs}(t) = G_{ij}^{ante}(t)e^{i(\phi_i(t)-\phi_j(t))} \int_{-\infty}^{\infty} \int_{-\infty}^{\infty} \mathcal{A}_\nu(l, m) I_\nu(l, m) e^{-2\pi i[u_{ij}(t)l+v_{ij}(t)m]} dl dm. \quad (2.56)$$

For the calibrators the true visibility is already known (i.e, well modelled), say  $V_{ij}(t)$ . So, if we divide the observed visibility of the calibrator,  $V_{ij}^{obs}(t)$ , with the known true visibility, then one can determine the gain factor,  $G_{ij}^{ante}(t)e^{i(\phi_i(t)-\phi_j(t))}$ . During observation, we inter-sparse the observation of the target source with observations of the calibrator. Once the gain solutions are determined during the observation scans on the phase calibrators with necessary solution interval, we can interpolate in time between the calibrator scans, i.e. on the target source.

#### 2.2.4.4 Bandpass Calibration

To handle changes of antenna gain with frequency, we can consider the baseline-based complex to be a function of frequency as  $G_{ij}(\nu)$ . For the frequency depended part we can write,

$$\begin{aligned} G_{ij} &\Rightarrow G_{ij}(t, \nu) = g_i(t, \nu)g_j^*(t, \nu) = [g_i(t)g_i(\nu)][g_j(t)g_j(\nu)]^* \\ &= (g_i(t)g_j^*(t))(g_i(\nu)g_j^*(\nu)) = G_{ij}(t)G_{ij}(\nu). \end{aligned} \quad (2.57)$$

Compensating for the change of gain with frequency is called *bandpass calibration*. During the process of calibration we have determined the values of  $G_{ij}(t)$  for a particular frequency channel (channel zero). Bandpass essentially determines the response of the interferometer across the band and hence determines the  $G_{ij}(\nu)$  for all the channels. This can be done by observing a strong calibrator source (in our case - the phase calibrator), whose spectrum is flat over the bandwidth of interest. The true visibility for this source is identical in all channels, the complex correlator-based gain,  $G_{ij}(\nu_k)$ , for the  $i - j$  baseline and the  $k^{th}$  frequency channel can be determined. With similar argument as for Equation 2.56, the frequency based gains can be determined by dividing the observed visibility,  $V_{ij}^{obs}(\nu_k)$  by the correct visibility,  $V_{ij}(\nu_k)$ .

#### 2.2.4.5 Deconvolution and Clean

- Dirty Beam and Dirty Image

We have seen in Equation 2.49, that the sky brightness distribution and the visibility are Fourier transforms of each other. But, the visibility function is not measured for all  $(u, v)$ s. Figure 2.16 shows the unfilled  $(u, v)$ , which were otherwise desired to determine the true sky brightness.

The GMRT UV-coverage at 610 MHz for ~4 hrs. 30 mins.  
V vs U for the Source:NGC2403

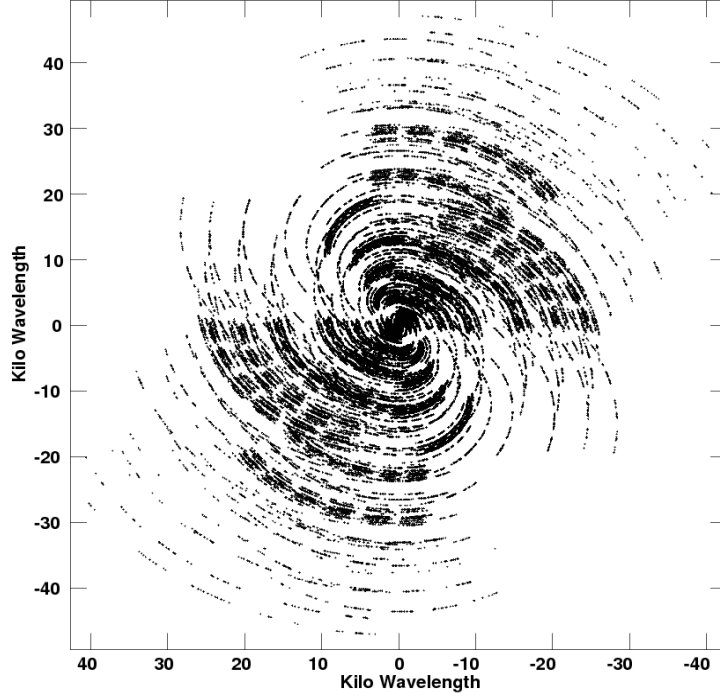


FIGURE 2.16: The UV coverage is shown for the the source NGC2403 observed at 610 MHz by GMRT.

So, the measured visibility is not really the Fourier transform of the true sky distribution. In the simplest case we can define a sampling cum weighting function,  $S(u, v)$ , such that, it is zero wherever there are no measurements and unity wherever  $(u, v)$  is measured. Therefore, the limited visibility can be written as the product of the desired true visibility,  $V(u, v)$ , and this function. That is,  $V_\nu^{measured}(u, v) = V_\nu(u, v)S(u, v)$ . In the Fourier domain, i.e. the sky, this multiplication is a convolution. Thus,

$$\begin{aligned} \mathcal{FT}[V_\nu^{measured}(u, v)] &= \mathcal{FT}[V_\nu(u, v)S(u, v)] = \mathcal{FT}[V(u, v)] \otimes \mathcal{FT}[S(u, v)], \\ \text{or } I_\nu^D(l, m) &= I_\nu(l, m) \otimes B^D(l, m). \end{aligned} \quad (2.58)$$

This discretely sampled sky brightness,  $I_\nu^D(l, m)$  is referred to as the dirty image or map. The Fourier transform of the weighting function,  $\mathcal{FT}[S(u, v)] = B^D(l, m)$ , is known as the dirty beam. In order to obtain the correct sky brightness,  $I_\nu(l, m)$ , one needs to deconvolve the dirty beam. The dirty beam is plagued with strong sidelobes and other undesirable effects and thus makes the interpretation of a dirty image extremely difficult. Mathematically, deconvolution of the Equation 2.58 to determine  $I_\nu(l, m)$  is not possible. Therefore, one resorts to the technique of reweighing the sampling function to interpret the  $I_\nu(l, m)$  in a better way. Let



us look at a simple example to demonstrate this. Let, the sampling function be,  $S(u, v) = 1$  within a disk of radius  $bmax$ . Here,  $bmax$  is the maximum baseline in the units of wavelength. The Fourier transform of this disk-like weighting function is the famous Airy disk. The beam could be cleaned up further by making the weighting non-uniform. We can taper the function to zero near the edge  $|(u, v)| = bmax$ . This tapering can be done by approximating the weight by a Gaussian. The sky is therefore convolved by the Fourier transform of this Gaussian, which is again a Gaussian. This makes the dirty image more cleanly related to the true map. The measurements are discrete and can be described by a sampling function,  $S(u, v)$ , which becomes zero wherever there are no measurements. Now, we can write down the equations for the dirty image formally. Invoking the sampling function to Equation 2.49, we get,

$$I_{\nu}^D(l, m) = \int \int V_{\nu}(u, v) S(u, v) e^{2\pi i(ul+vm)} du dv. \quad (2.59)$$

As discussed above, the dirty beam is the Fourier transform of the sampling function. Thus,

$$B^D(l, m) = \int S(u, v) e^{2\pi i(ul+vm)} dl dm. \quad (2.60)$$

- The CLEAN Algorithm The CLEAN algorithm developed by J. Högbom (1974), was one of the first attempts to deconvolve the dirty beam from the true map. This is a simple iterative approach to find out the position and strengths of, predominantly, point sources in the sky. The iterations operates in the map plane and uses a known shape of dirty beam to distinguish between real structure and sidelobe disturbances on the dirty map.

1. Högbom CLEAN From Equation 2.58 we have seen that, the dirty image is a convolution of dirty beam and the true sky brightness. This process of CLEAN is an image plane based algorithm. Let us assume the sky contains isolated point sources. This implies, in the dirty map, we would see dirty beams at the position of each source and are scaled by the strength of the source present at that position. Now, the position and the strength of the strongest source is identified. One can search for the peaks at limited areas in the image, called the CLEAN windows, instead of considering the entire image. Then at the positions of the peaks in the dirty image, relevantly scaled dirty beam is subtracted. In practice one does not subtract the entire dirty beam, but subtracts it with a gain factor,  $\gamma \leq 1$ , which is termed as the loop gain. The position and amplitude of the point source subtracted is recorded in a model. This process of identifying peaks and subtracting is continued until we are left with what is called the residual. The accumulated

point source model is then convolved with an idealised CLEAN beam and are added back to the residual.

2. Clark (or BGC) CLEAN This is a FFT-based CLEAN algorithm developed by B. G. Clark (1980). In this process of CLEAN there are two cycles, termed as the minor cycle and the major cycle. Firstly, the UV data are gridded according to the requirements to carry the FFT. All the measurements within the grid are represented by their vector average (with relevant weights) placed at the center of the grid. Then the dirty beam is calculated by taking the Fourier transform of this gridded sampling function. Then the minor cycle starts. It first selects a certain patch of the beam so that the highest exterior sidelobes are included. Then points are selected from the dirty image whose intensity is greater than the highest exterior sidelobe of the beam. In this process we can choose multiple peaks. For each peak Högbom CLEAN is performed using the beam patch and the selected points. Then the algorithm proceeds with the major cycle. Here, Fourier transform of the selected point source model is done multiplied by the weighted sampling function. The subtraction is then performed on the UV domain, i.e, unlike the Högbom CLEAN, it is done in the Fourier domain of the gridded UV data. Once we are left with noise like data in the UV domain, we restore back the CLEANed components.
3. Cotton-Schwab CLEAN In 1984, Cotton and Schwab (Schwab, 1984) developed a variant of the Clark CLEAN algorithm. This was basically a DFT-based CLEAN algorithm. Unlike the Clark algorithm, the major cycle subtraction of the CLEANed peak components are done on the ungridded visibility data. This makes sure that the subtraction is performed on a data which is free from interpolation and weighting noise, which was otherwise present during the gridding for FFT. It also has the ability to image and CLEAN several fields simultaneously. In minor cycle each field is CLEANed independently, but in the major cycle, CLEAN components from all the fields are removed. This is of great help while imaging wide fields and correcting for the w-term.
4. SDI CLEAN All the CLEANing algorithm discussed above works extremely well for sources that are point-like. But, if the source is structured and extended, then each point in the source are treated as a separate point source and the algorithm proceeds. This tends to make the final map clumpy, which was otherwise a smooth source. Steer, Dewdney and Ito (1984) developed an algorithm which works well with extended structures. This process of CLEAN avoids the spike-like samples of peak components by cutting off the

top of a plateau of emission found in the residual image(s) in a relatively uniform way. This algorithm converges well for extended sources.

#### 2.2.4.6 Self-Calibration

- The need of Self-Calibration:

The main drawback to ordinary calibration arises from temporal and spatial variations in the atmosphere (troposphere and ionosphere) through which the wavefront passes before reaching the array elements. Values for the  $g_i(t)$  inferred from a calibration source may not apply to the source observed at a different time and in a different part of the sky. Hence the effect of  $g_i(t)$  cannot be removed completely, and residual errors remain. The level of error varies tremendously with the frequency at which the observation are made and with the lengths of the baselines involved. Other obstacles to ordinary calibration are the strength of the calibrators, and any resolved structure they may contain. In some circumstances one may not be able to find a sufficiently strong unresolved calibration source anywhere near the source of interest. Fortunately, progress can be made if the element gains are allowed to be degrees of freedom when determining the sky intensity distribution. Allowing the element gains to be free parameters is the basic principle of self-calibration.

## 2.3 Fundamentals of Radiative Transfer

### 2.3.1 Specific Intensity

If  $dE$  is the amount of radiant energy which crosses the area  $dA$  in time  $dt$  with unit normal  $\hat{n}$  in a direction within solid angle  $d\Omega$  centered about  $\hat{k}$  and with photon frequency between  $\nu$  and  $\nu + d\nu$ , then the monochromatic specific intensity  $I_\nu$  is defined by the equation:

$$dE = I_\nu(\hat{\mathbf{k}}, \mathbf{x}, t) \hat{\mathbf{k}} \cdot \hat{\mathbf{n}} dA d\Omega d\nu dt. \quad (2.61)$$

The quantity  $I_\nu$  has the CGS units  $[I_\nu] = \text{erg cm}^{-2} \text{s}^{-1} \text{Hz}^{-1} \text{steradians}^{-1}$ . The rationale for this definition comes from the conservation of  $I_\nu$  in the absence of interactions with matter. The total time derivative of  $I_\nu(\hat{\mathbf{k}}, \mathbf{x}, t)$  gives,

$$\frac{\partial I_\nu}{\partial t} + c\hat{\mathbf{k}} \cdot \nabla I_\nu = \text{source} - \text{sinks}. \quad (2.62)$$

### 2.3.2 Equation of Radiative Transfer

The transport Equation 2.62 is preferably written per unit length rather than per unit time as,

$$\frac{1}{c} \frac{\partial I_\nu}{\partial t} + \hat{\mathbf{k}} \cdot \nabla I_\nu = \frac{1}{4\pi} \rho j_\nu^{spont} - \rho k_{\nu effective}^{abs} I_\nu - \rho k_\nu^{sca} I_\nu + \rho k_\nu^{sca} \oint \phi(\hat{\mathbf{k}}, \hat{\mathbf{k}}') I_\nu(\hat{\mathbf{k}}') d\Omega'. \quad (2.63)$$

where,

$\rho \rightarrow$  mass density per unit volume of the gas,

$j_\nu \rightarrow$  emissivity per unit mass,

$k_{\nu effective}^{abs} \rightarrow$  total absorption opacity,

$k_\nu^{sca} \rightarrow$  total scattering opacity,

$\phi(\hat{\mathbf{k}}, \hat{\mathbf{k}}') \rightarrow$  scattering probability density (from  $\hat{\mathbf{k}}'$  to  $\hat{\mathbf{k}}$ ).

The effect of stimulated emission is taken into account in the  $k_{\nu effective}^{abs}$  term as,

$$k_{\nu effective}^{abs} = k_\nu^{abs} - j_\nu^{induced}. \quad (2.64)$$

The last term in Equation 2.63 satisfies the normalization and reversibility constraints:

$$\oint \phi(\hat{\mathbf{k}}, \hat{\mathbf{k}}') d\Omega' = 1 = \oint \phi(\hat{\mathbf{k}}, \hat{\mathbf{k}}') d\Omega. \quad (2.65)$$

In the RHS of Equation 2.63,

$\rho j_\nu^{spont}$  represents the source for radiation that comes from true emission (the term is reduced by a factor of  $4\pi$  to make it per steradians);

$\rho k_{\nu effective}^{abs}$  represents the amount of light removed from the beam, per unit length of photon travel, by the effects of true absorption corrected for stimulated emission;

$\rho k_\nu^{sca}$  represents the analogous amount scattered out of the relevant beam;

$\oint \phi(\hat{\mathbf{k}}, \hat{\mathbf{k}}') I_\nu(\hat{\mathbf{k}}, \hat{\mathbf{k}}') d\Omega'$  represents the integral contribution scattered into the beam from any other line of sight.

### 2.3.3 Solution of the Radiative Transfer Equation and Optical Depth

If light travels across an object in interval which is short compared with its evolutionary time, then the time-dependence can be ignored in the corresponding problem of radiation transport. Thus the Equation 2.63 can be written as

$$\hat{\mathbf{k}} \cdot \nabla I_\nu + \rho k_\nu I_\nu = \rho \left( \frac{j_\nu^{spont}}{4\pi} + k_\nu^{sca} \Phi_\nu \right), \quad (2.66)$$

where  $k_\nu = k_{\nu_{effective}}^{abs} + k_\nu^{sca}$  is the total opacity and  $\Phi_\nu(\hat{\mathbf{k}}', \mathbf{x}) = \oint \phi(\hat{\mathbf{k}}, \hat{\mathbf{k}}') I_\nu(\hat{\mathbf{k}}, \mathbf{x}) d\Omega'$  is the intensity weighted by the angular phase for scattering.

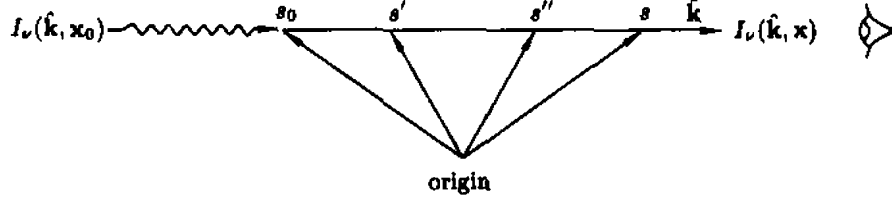


FIGURE 2.17: Geometry for ray-path integration for  $I_\nu$ .

In case of absorption we neglect  $\rho j_\nu^{spont}/4\pi$  i.e. the emission term, and  $\Phi_\nu(\hat{\mathbf{k}}', \mathbf{x}) = 0$ , then the Equation of radiative transfer 2.66 becomes,

$$\begin{aligned} \hat{\mathbf{k}} \cdot \nabla I_\nu &= -\rho k_\nu I_\nu, \\ \frac{dI_\nu}{dS} &= -\rho k_\nu I_\nu. \end{aligned} \quad (2.67)$$

Now, defining the optical depth as,

$$d\tau_\nu = \rho k_\nu dS, \quad \text{or} \quad \tau_\nu = \int \rho k_\nu dS. \quad (2.68)$$

Therefore,

$$\begin{aligned} \frac{dI_\nu}{I_\nu} &= -d\tau_\nu, \\ \ln I_\nu &= -\tau_\nu + c. \end{aligned} \quad (2.69)$$

At  $\tau_\nu = 0$ ,  $I_\nu = I_0$ , then,  $c = \ln I_0$ , substituting in above Equation,

$$\begin{aligned} \ln I_\nu - \ln I_0 &= -\tau_\nu. \\ \text{Thus, optical depth is } \tau_\nu &= -\ln \left( \frac{I_\nu}{I_0} \right). \end{aligned} \quad (2.70)$$

## 2.4 Neutral Hydrogen

### 2.4.1 HI 21-cm Emission and Absorption

The ISM is composed primarily of hydrogen, and atomic hydrogen can be conveniently detected and studied via the 21-cm line, originating in the hyperfine splitting of the 1s electronic ground state of hydrogen. Studies of this line have allowed mapping of the distribution of HI in the Milky Way and other galaxies, determination of the galactic rotation curve, and measurement of the gas temperature in interstellar clouds.

### 2.4.2 Spin temperature

The electron in the electronic ground state (1s) of atomic hydrogen can have its spin either parallel or antiparallel to the spin of the proton as shown in Figure 2.18. The coupling of the electron's magnetic moment to the magnetic field produced by the magnetic moment of the proton results in "hyperfine splitting" of the parallel and antiparallel spin states. The antiparallel spin state (with degeneracy  $g = 1$ ) has the lower energy, which we take to be  $E_l = 0$ . The parallel spin state (with total spin  $S = 1$ , and degeneracy  $g = 2S + 1 = 3$ ) has an energy  $E_u - E_l = 5.87 \times 10^{-6} eV$ . When the electron drops to the ground state, the electron spin flips, and a photon is emitted with a wavelength  $\lambda = 21.11$  cm.

Because of the small energy splitting between these two spin states, the cosmic microwave background by itself is able to populate the upper level. For all conditions of interest (at least until the expansion factor of the universe increases by a factor 100), we expect the excitation temperature (or "spin temperature")  $T_{exc} \equiv T_{spin} \gg \frac{h\nu}{k} i.e. T_{spin} \gg 0.0682$  K, and

$$\frac{n_u}{n_l} \equiv \frac{g_u}{g_l} e^{-\frac{h\nu_{ul}}{kT_{spin}}}. \quad (2.71)$$

$$\text{As } \frac{g_u}{g_l} = 3, \quad \frac{n_u}{n_l} = 3e^{-\frac{0.0682K}{kT_{spin}}} \approx 3.$$

$$\text{Now,} \quad n(\text{HI}) = n_u + n_l = n_u \left(1 + \frac{1}{3}\right) = \frac{4}{3}n_u. \quad (2.72)$$

$$\text{Thus} \quad n_u = \frac{3}{4}n(\text{HI}) \quad \text{and} \quad n_l = \frac{1}{4}n(\text{HI}).$$

Because the upper level contains  $\sim 75\%$  of the HI under all conditions of interest, the HI 21-cm emissivity is effectively independent of the spin temperature.

The emissivity  $j_\nu$  is defined as the power radiated per unit frequency per unit solid angle per unit volume.

$$j_\nu = n_u \frac{A_{ul}}{4\pi} h\nu_{ul} \phi_\nu \approx \frac{3}{16\pi} A_{ul} h\nu_{ul} n(\text{HI}) \phi_\nu. \quad (2.73)$$

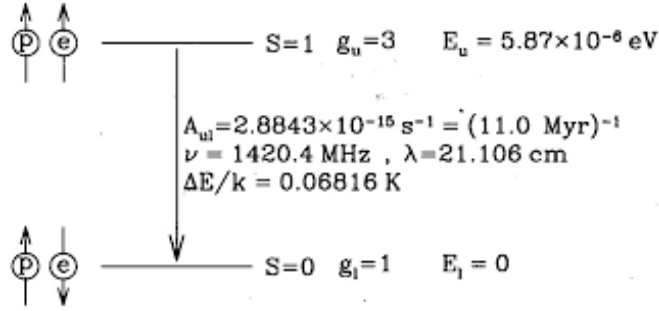


FIGURE 2.18: Hyperfine splitting of the 1s ground state of atomic Hydrogen.

where  $\phi_\nu$  is the normalized line profile ( $\int \phi_\nu = 1$ ), determined by the velocity distribution of the HI.

The attenuation coefficient  $k_\nu$  is proportional to the net absorption i.e. true absorption minus stimulated emission,

$$\begin{aligned}
 k_\nu &= n_l \sigma_{lu} - n_u |\sigma_{ul}|, \quad \text{where } n_l, n_u \rightarrow \text{number density of lower and upper state,} \\
 &= n_l \frac{g_u}{g_l} \frac{c^2}{8\pi\nu_{lu}^2} A_{ul} \phi_\nu - n_u \frac{c^2}{8\pi\nu_{ul}^2} A_{ul} \phi_\nu, \\
 &= n_l \frac{g_u}{g_l} \frac{A_{ul}}{8\pi} \lambda_{ul}^2 \phi_\nu \left( 1 - \frac{n_u g_l}{n_l g_u} \right), \\
 &= n_l \frac{g_u}{g_l} \frac{A_{ul}}{8\pi} \lambda_{ul}^2 \phi_\nu (1 - e^{-h\nu_{ul}/kT_{spin}}).
 \end{aligned} \tag{2.74}$$

As  $e^{-h\nu_{ul}/kT_{spin}} \approx 1$ , for  $T_{spin} \gg \frac{h\nu}{k}$  the correction for stimulated emission is very important and cannot be neglected. Now  $h\nu_{ul}/kT_{spin} \ll 1$  for all conditions of interest,  $e^{-h\nu_{ul}/kT_{spin}} \approx 1 - h\nu_{ul}/kT_{spin}$ , therefore substituting in above Equation,

$$\begin{aligned}
 k_\nu &\approx \frac{1}{4} n(\text{HI}) \frac{3}{1} \frac{A_{ul}}{8\pi} \lambda_{ul}^2 \phi_\nu \left( \frac{h\nu_{ul}}{kT_{spin}} \right), \\
 &\approx \frac{3}{32\pi} A_{ul} \left( \frac{hc\lambda_{ul}}{kT_{spin}} \right) n(\text{HI}) \phi_\nu.
 \end{aligned} \tag{2.75}$$

Thus, the attenuation coefficient  $k_\nu \propto 1/T_{spin}$ .

Suppose that HI has a Gaussian velocity distribution then,

$$\phi_\nu = \frac{1}{\sqrt{2\pi}} \frac{c}{\nu_{ul}} \frac{1}{\sigma_V} e^{-u^2/2\sigma_V^2}. \tag{2.76}$$

and the attenuation coefficient is,

$$\begin{aligned}
 k_\nu &= \frac{3}{32\pi} A_{ul} \left( \frac{hc\lambda_{ul}}{kT_{spin}} \right) n(\text{HI}) \frac{1}{\sqrt{2\pi}} \frac{c}{\nu_{ul}} \frac{1}{\sigma_V} e^{-u^2/2\sigma_V^2}, \\
 &= 2.19 \times 10^{-19} \text{ cm}^2 n(\text{HI}) \left( \frac{K}{T_{spin}} \right) \left( \frac{\text{km s}^{-1}}{\sigma_V} \right) e^{-u^2/2\sigma_V^2}.
 \end{aligned} \tag{2.77}$$

The optical depth is,

$$\begin{aligned}
 \tau_\nu &= \int k_\nu dS, \\
 \tau_\nu &= 2.19 \times 10^{-19} \text{ cm}^2 \left( \frac{K}{T_{spin}} \right) \left( \frac{\text{km s}^{-1}}{\sigma_V} \right) e^{-u^2/2\sigma_V^2} \int n(\text{HI}) .dS, \\
 \tau_\nu &= 2.19 \left( \frac{N(\text{HI})}{10^{21} \text{ cm}^{-2}} \right) \left( \frac{100K}{T_{spin}} \right) \left( \frac{\text{km s}^{-1}}{\sigma_V} \right) e^{-u^2/2\sigma_V^2}.
 \end{aligned} \tag{2.78}$$

where  $N(\text{HI}) \equiv \int n(\text{HI}) .dS$  is the column density of HI.

Therefore the spin temperature is given by,

$$\left( \frac{T_{spin}}{100K} \right) = 2.19 \left( \frac{N(\text{HI})}{10^{21} \text{ cm}^{-2}} \right) \left( \frac{1}{\tau_\nu} \right) \left( \frac{\text{km s}^{-1}}{\sigma_V} \right) e^{-u^2/2\sigma_V^2}. \tag{2.79}$$



## Chapter 3

# Data Analysis and Calculations

### 3.1 Data Reduction using AIPS

- Our source which is a quasar-galaxy pair (QGP) J1443+0214 was observed with GMRT on 2012 June 2. This quasar is one them from the sample of quasars obtained through an optical survey on the basis of strong MgII absorption in their continuum. The bandwidth used was 4.17 MHz split into 512 spectral channels, centered on the redshifted 21-cm frequency of foreground galaxy. The foreground galaxy in this QGP is identified by the detection of emission lines in the SDSS spectrum of QSO. The foreground galaxy is invisible otherwise.
- We reduce the data of this QGP obtained from GMRT archive using AIPS (Astronomical Image Processing System) software. The steps in spectral-line data reduction are as follows:
  1. Loading the data
  2. Flagging and Editing
  3. Calibration - Gain Calibration, Bandpass Calibration
  4. Splitting the target source data
  5. Making and Cleaning the image
  6. Self-Calibration
  7. Imaging for making a model for continuum subtraction
  8. Obtaining the final spectrum

### 3.1.1 Glimpses of data reduction process in AIPS

- The Figure 3.1 shows a screenshot of a visibility plot, which is plotted using task ‘VPLOT’ in order to look at the amplitude and phase variations of all sources with time.

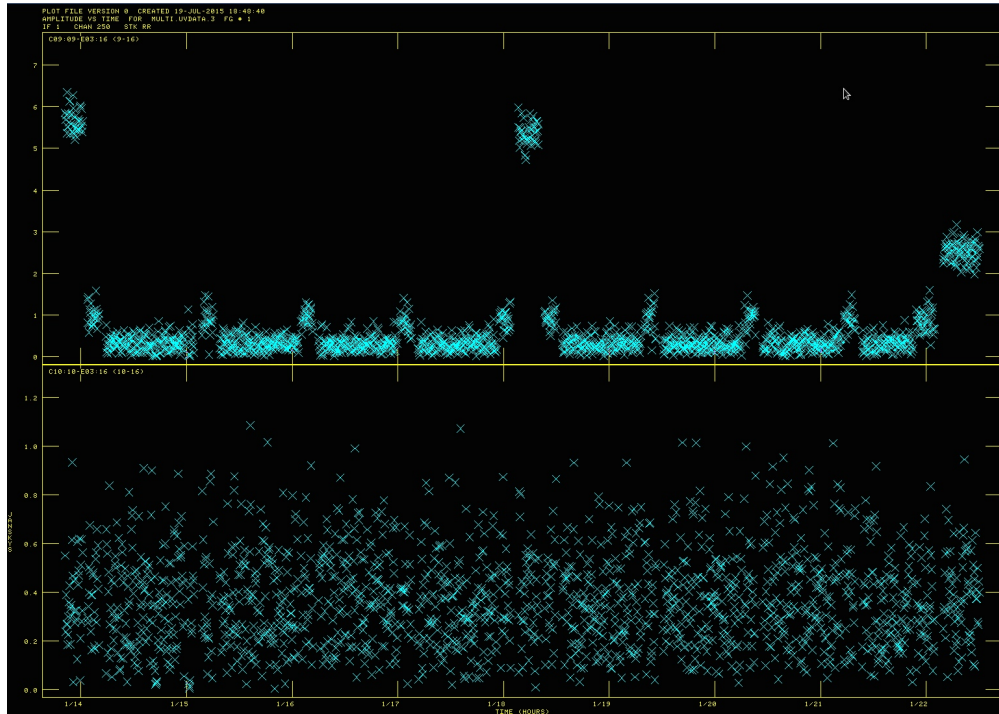


FIGURE 3.1: Plot of Flux (Janskys) and Time (Hours) for source J1443+0214 for channel:250, baseline:09 - 16 (above) and 10 - 16 (below).

The bad data is identified from such plots, like in Figure 3.1 the whole timerange for baseline:10 - 16 is bad because none of the 3 sources observed are identifiable. Further, primary flagging of bad data is done using task ‘UVFLG’. Before that a ‘good channel’ is chosen by looking at the plots so as to use it as a reference for further process.

- The Figure 3.2 shows the image of our source J1443+0214 formed by task ‘IMAGR’ after completing gain calibration and bandpass calibration but before starting self-calibration.

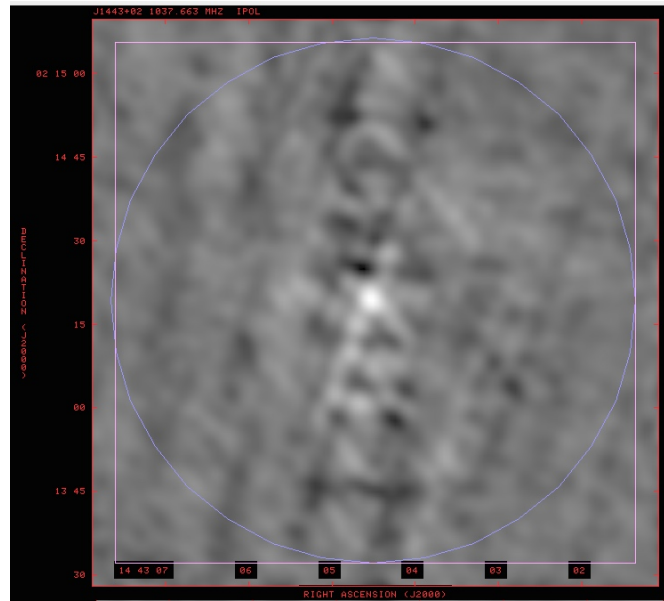


FIGURE 3.2: Image of source J1443+0214 before self-calibration.

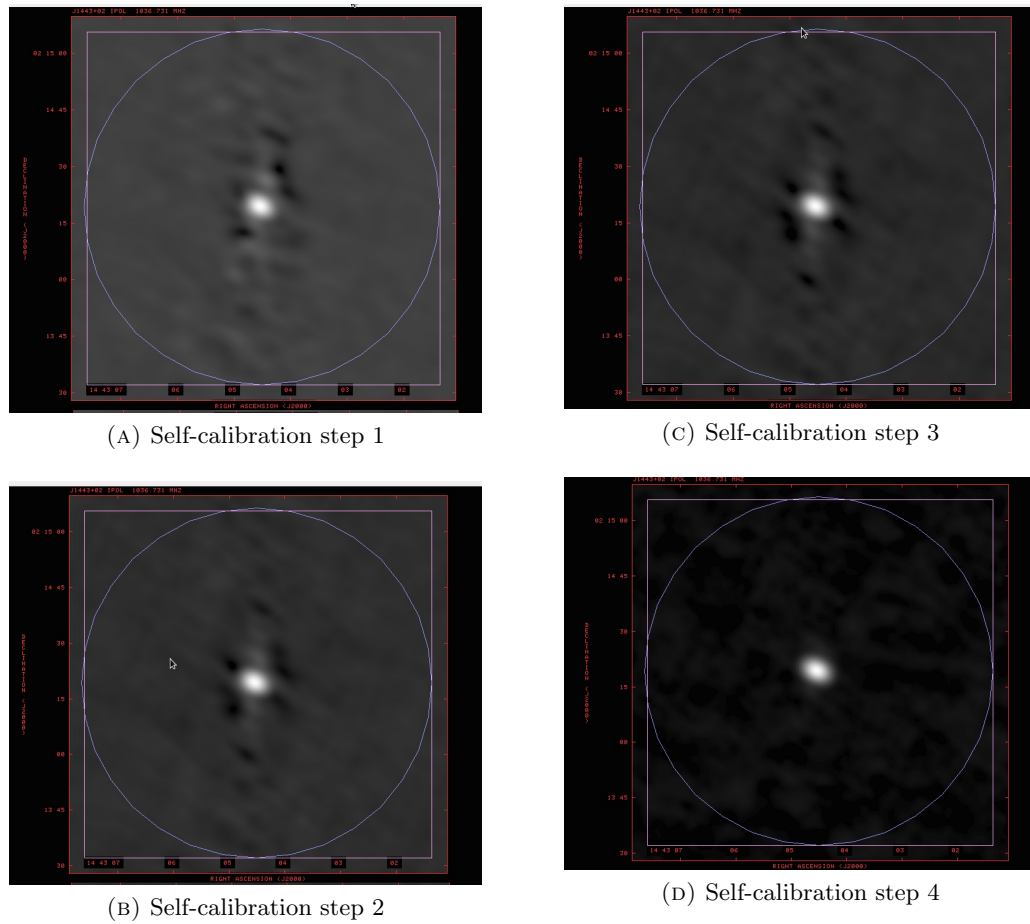


FIGURE 3.3: Step by step cleaning of image during self-calibration.

- The Figure 3.3 shows the step by step process of cleaning of the source image during self-calibration, where the final image D shows reduced noise as compared to image A.

- The Figure 3.4 shows the spectrum of the source obtained by running task ‘ISPEC’ on the spectral data cube.

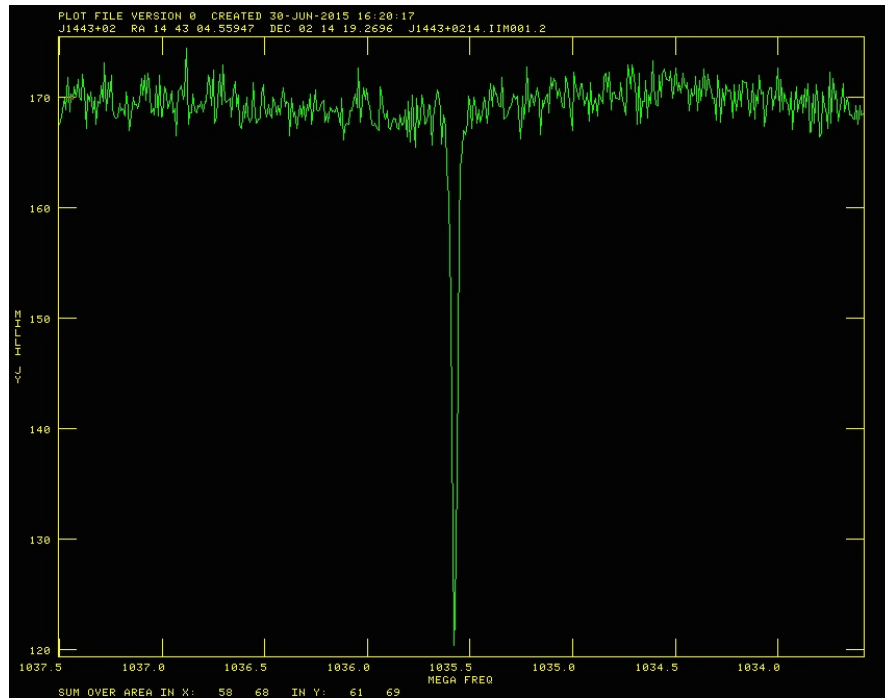


FIGURE 3.4: The spectrum of J1443+0214 obtained at  $z_{abs} = 0.37$ , showing prominent 21-cm absorption line.

We extract the amplitude and frequency data for each point in this spectrum to further process it using Interactive Data Language (IDL).

### 3.2 Gaussian fitting and Calculations using IDL

- We again obtain the spectrum of the source using IDL from the data extracted through AIPS. Firstly we fit a gaussian profile to the continuum and then divide our spectrum with this continuum. Then we fit another gaussian profile to the spectral line and determine the peak optical depth using Equation 2.70. Thus the peak optical depth calculated is  $\tau_\nu^{peak} = 0.3249$ .

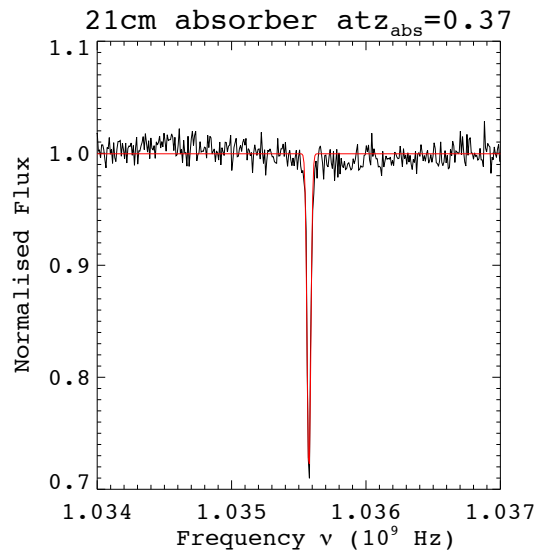


FIGURE 3.5: Gaussian fitting to the absorption line profile.

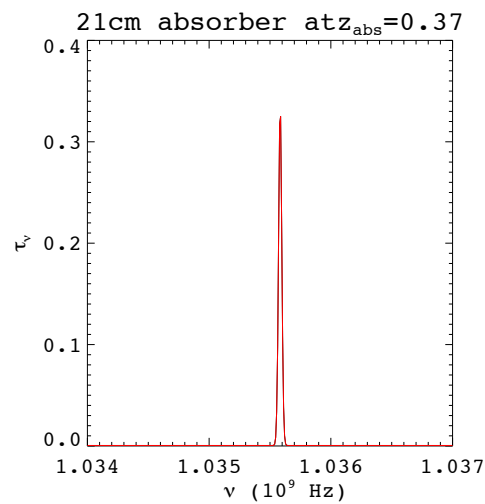


FIGURE 3.6: Optical depth  $\tau_\nu$  of HI obtained from the spectrum.

- The FWHM of fitted gaussian is  $32667.941 Hz \equiv 9.4637 km s^{-1}$  and thus,  $\sigma_V$  is calculated from the equation as,

$$\begin{aligned}\sigma_V &= \frac{\text{FWHM}}{2\sqrt{2\ln 2}} = \frac{\text{FWHM}}{2.354} \\ &= \frac{9.4637}{2.354} \\ &= 4.0188\end{aligned}\tag{3.1}$$

- Using  $N(\text{HI}) = 8 \times 10^{21} \text{ cm}^{-2}$  from Gupta et al. (2013), and substituting  $\sigma_V = 4.0188$  and  $\tau_V^{peak} = 0.3249$  obtained above, we calculate the spin temperature of HI from Equation 2.79. As for peak optical depth,  $u = 0$ , Equation 2.79 becomes,

$$\begin{aligned}\left(\frac{T_{spin}}{100K}\right) &= 2.19 \left(\frac{N(\text{HI})}{10^{21} \text{ cm}^{-2}}\right) \left(\frac{1}{\tau_V^{peak}}\right) \left(\frac{km s^{-1}}{\sigma_V}\right) \\ \left(\frac{T_{spin}}{100K}\right) &= 2.19 \left(\frac{8}{10^{21} \text{ cm}^{-2}}\right) \left(\frac{1}{0.3249}\right) \left(\frac{km s^{-1}}{4.0188}\right)\end{aligned}\tag{3.2}$$

$$T_{spin} = 1338.81K,$$

where we assumed the covering factor to be unity.

## Chapter 4

# Results and Future work

In this project we have searched for the possible associations of 21-cm cool HI gas with MgII absorber at  $z_{\text{abs}} = 0.3714$ . In this regard, we have searched for 21-cm absorption line using GMRT observations. The summary of our results is as follows:

- We found 21-cm absorption line at the redshift of MgII absorber  $z_{\text{abs}} = 0.37$ .
- Detection of 21-cm absorption line indicates that this MgII absorber may be associated with a galaxy possessing cool gas and hence may be in the phase of ongoing star formation.
- We estimated the  $T_{\text{spin}}$  based on the observed  $\tau_{\nu}$  (HI) to be 1338.81 K by using  $N(\text{HI}) = 8 \times 10^{21} \text{ cm}^{-2}$  from the literature .

In future, we would like to extend our investigation for similar other probable cases along with the multi-wavelength data to constrain the physical conditions prevailing in such high redshift protogalaxies.



## Chapter 5

## References

1. Synthesis Imaging in Radio Astronomy II, Edited by G. B. Taylor, C. L. Carilli, R. A. Perley.
2. N. Gupta, R. Srianand, P. Noterdaeme, P. Petitjean, and S. Muzahid, 2013 Astronomy and Astrophysics: 21-cm absorption from galaxies at  $z \sim 0.3$ .
3. The Physics of Astrophysics, Volume I, Radiation, Frank H. Shu.
4. Princeton Series in Astrophysics: Physics of the Interstellar and Intergalactic Medium, Bruce T. Draine.
5. AIPS Cookbook, The National Radio Astronomy Observatory.
6. Data Analysis Using AIPS, Sambit Roychowdhury (NCRA-TIFR)
7. An easy guide to GMRT data analysis using AIPS, Neeraj Gupta, (IUCAA)
8. Behind AIPS, Aritra Basu (NCRA-TIFR)

# Appendix A

## Introduction to AIPS

### A.1 Introduction

The NRAO Astronomical Image Processing System (AIPS) is a software package for interactive calibration and editing of radio interferometric data and for the calibration, construction, display and analysis of astronomical images made from those data using Fourier synthesis methods.

AIPS is the principal tool for display and analysis of both two-dimensional and three-dimensional radio images.

It contains facilities for display and editing of data in the aperture, or uv plane; for image construction by Fourier inversion; for deconvolution of the point source response by Clean; for image combination, filtering, and parameter estimation; and for a wide variety of image and graphical displays.

The AIPS system consists of several distinct parts. When using the AIPS system, you talk to your computer through a command processor called POPS (People Oriented Parsing System) that lives in the program AIPS. This program interacts with the user, performs many of the display functions, does some manipulation of data and initiates other programs which run asynchronously from AIPS.

Functions built into AIPS are called verbs, the asynchronous programs are called tasks, and both are controlled by the values of parameters in the POPS processor known as adverbs.

## A.2 Tasks

AIPS provides a way for you to set up the parameters for, and then execute, many applications programs sequentially or in parallel. The more computationally intensive programs may take many minutes, hours (or even days) of CPU time to run to completion. They are therefore embodied in AIPS “tasks” programs that are spawned by the AIPS program to execute independently and asynchronously.

When a task is initiated from AIPS an external file is read which specifies the number and order of adverbs whose values are sent to the task. These values, along with some “hidden” values, are written into a disk file. AIPS then initiates the requested task and suspends itself indefinitely. The task reads the disk file and depending on the value of a logical “hidden” adverb it may resume AIPS. The task then does the requested operation and before stopping resumes AIPS if this was not done previously. The task sends AIPS a return code when AIPS is resumed. Tasks are used for operations which either require much computer memory or CPU time or both, whereas verbs are used for operations which take no longer than a few seconds to finish. Since the tasks run asynchronously from AIPS, the user may do other things while one or more tasks are running.

## A.3 Verbs

Verbs are the functions built into the AIPS program itself. Verbs are the magic words which cause FORTRAN code to execute some function. They are compiled into AIPS by the programmers and their meaning remains fixed. Many of these involve the display of images and most of the interactive features of the AIPS system. Some of the smaller AIPS utilities run quickly enough to be run inside the AIPS program rather than being spawned. These “verbs” include simple arithmetic and POPS operations, the HELP, ABOUT, INP, and GO commands, and many more. Verbs are sent into action simply by setting their input parameters and typing the name of the verb followed by enter. While a verb is executing, AIPS will not respond to anything you type on the terminal.

## A.4 Adverbs

AIPS uses “adverbs” (which may be real numbers or character strings, scalars or arrays) to pass parameters to both “verbs” and “tasks.” Adverbs are the symbols used to address values. Many AIPS tasks will assume sensible “default” values for adverbs that you

choose not to specify. Some adverbs cannot be sensibly defaulted; these should be clearly indicated in the appropriate help information. You may review the current input parameters for any AIPS task or verb by using pseudoverb INP.

**>inp**                                   to review the parameters for task TASK, or  
**>inp task name**                   to review the adverbs for task task name

## A.5 AIPS message file

AIPS and all tasks talk back to you by writing messages to a disk file called the “message file” and/or by sending them to you on the appropriate “message monitor”. Simple instructions and progress messages usually go only to the monitor; very few messages go only to the file. For AIPS itself, the message monitor is always the workstation window or terminal into which you are typing your commands. For details enter

**>help msgsrv**

At most AIPS installations, you get a message server by default. You may also control the size and appearance of the message server with parameters in the X-Windows.Xdefaults file. These parameters are also listed in by help msgsrv.

You may review the contents of the message file by using the verb PRTMSG.

**>prtmsg**

PRTMSG does not delete messages from your message file.

To delete messages and to compress the message file use the verb CLRMSG.

**>clrmsg**

## A.6 Data files and Catalogues

Data is kept in files which are catalogued in AIPS. At present we have two kinds of data (more are possible): images and uv data. The internal structure is much like that of a FITS (Flexible Image Transport System) format tape except that the data may be in floating point format. Associated with each main data file may be up to 10 types of auxiliary information files with up to 255 versions of each type. The basic information about the main data file and the existence of the auxiliary files (called extension files) is kept in a catalog file. Bookkeeping and other information is kept in the first record of most of the extension files. One example of the extension file is the History file in which

a record of the processing of the data is automatically logged by the AIPS tasks. The catalogue header record is used to keep various pieces of information about the data in the main data file and keeps track of the number and types of extension files associated with the main data file. AIPS data files have a structure very similar to the structure of data of FITS format tapes. An image consists of a rectangular array of up to 7 dimensions. Pixels locations must be evenly spaced along each axis, although a proper redefinition of the axis can usually make this possible. The header record contains the number of pixels along each axis, a label for each axis, the number of the reference pixel, the coordinate at the reference pixel, the coordinate increment between pixels and the coordinate rotation. The axes of images may be in any order.

The User's UV catalog can be viewed by the verb UCAT (uc) and the Map catalog by verb MCAT (mc).

---

```
>uc
AIPS 1: Catalog on disk 1
AIPS 1: Cat Usid      Mapname   Class    Seq   Pt      Last access   Stat
AIPS 1:   1  501        UV       .QSO    .    1    UV       21-JUN-2015 10:25:40  READ
AIPS 1:   2  501   J1443+0214 .SPLIT.  1    UV       22-JUN-2015 16:50:14
AIPS 1:   3  501   J1443+0214 .SPLAT.  1    UV       25-JUN-2015 16:12:28
AIPS 1:   4  501   J1443+0214 .CALIB.  1    UV       21-JUN-2015 10:26:08
AIPS 1:   6  501        UV       .IMAGR.  1    UV       21-JUN-2015 10:26:31  WRIT
AIPS 1:   8  501   J1443+0214 .CALIB.  2    UV       21-JUN-2015 12:50:57
AIPS 1:  11  501   J1443+0214 .CALIB.  3    UV       21-JUN-2015 16:39:36
AIPS 1:  14  501   J1443+0214 .CALIB.  4    UV       21-JUN-2015 17:05:48
AIPS 1:  17  501   J1443+0214 .SPLIT.  2    UV       27-JUN-2015 16:14:02
AIPS 1:  20  501   J1443+0214 .UVSUB.  1    UV       24-JUN-2015 16:50:46
>mc
AIPS 1: Catalog on disk 1
AIPS 1: Cat  Usid      Mapname   Class    Seq   Pt      Last access   Stat
AIPS 1:   5  501   J1443+0214 .IBM001.  1    MA       20-JUN-2015 12:57:22
AIPS 1:   7  501   J1443+0214 .ICL001.  1    MA       21-JUN-2015 10:19:18
AIPS 1:   9  501   J1443+0214 .IBM001.  2    MA       20-JUN-2015 13:43:48
AIPS 1:  10  501   J1443+0214 .ICL001.  2    MA       21-JUN-2015 12:58:39
AIPS 1:  12  501   J1443+0214 .IBM001.  3    MA       21-JUN-2015 13:02:12
AIPS 1:  13  501   J1443+0214 .ICL001.  3    MA       21-JUN-2015 16:42:13
AIPS 1:  15  501   J1443+0214 .IBM001.  4    MA       21-JUN-2015 16:55:29
AIPS 1:  16  501   J1443+0214 .ICL001.  4    MA       21-JUN-2015 17:05:48
AIPS 1:  18  501   J1443+0214 .IBM001.  5    MA       21-JUN-2015 17:23:24
AIPS 1:  19  501   J1443+0214 .ICL001.  5    MA       27-JUN-2015 10:31:16
AIPS 1:  22  501   J1443+0214 .IBM001.  6    MA       23-JUN-2015 01:36:20
AIPS 1:  23  501   J1443+0214 .IIM001.  1    MA       26-JUN-2015 11:53:16
AIPS 1:  24  501   J1443+0214 .IBM001.  7    MA       27-JUN-2015 16:14:43
AIPS 1:  25  501   J1443+0214 .IIM001.  2    MA       30-JUN-2015 16:20:17
```

---

The uv data file in slot 1 is opened for READING. The IMAGR file is opened for WRITing. Procedures that attempt to read files which are opened for writing, or vice versa, will be rejected with appropriate error messages. You must therefore note any non-blank entries in the STAT column carefully. In some situations (mainly involving

system crashes or abortion of tasks files may be left in READ or WRIT status indefinitely. If this happens, you may reset the file status with CLRSTAT after issuing the appropriate INDISK and GETNAME.

**>indisk 1**

**>getn 6**

**>clrstat**

The verb GETNAME (n) will interpret its immediate argument as a catalog slot number and assign adverbs INNAME,INCLASS,INSEQ,etc. to correspond to that slot.

For example:

**>getn 1**

Got (1) disk = 1 user = 501 type= UV UV.QSO.1

To destroy any catalog entry file and all the associated extension files use the verb ZAP.

For example:

**>getn 20**

Got (1) disk = 1 user = 501 type=UV J1443+0214 .UVSUB . 1

**>zap**

Every image or uv data set in AIPS has an associated header file that contains information needed to describe the data set in detail. The header also contains information on the number of extension files of each type that have been associated with the data set. Multi-source uv data files may have many extensions. The most important are the HISTORY file, the ANTennas file (subarray geometric data, date, frequency and polarization information, etc.), the BP (bandpass) file for bandpass calibration data, the CL (calibration) file for calibration and model information, the FQ (frequency) file for frequency offsets of the different IFs, the FG (flag) file for editing information, the NX (index) file which assists rapid access to the data, the SN (solution) file for gain solutions from AIPS calibration routines, and the SU (source) file with source-specific information such as name, position, and velocity. The header information can be listed from the selected catalog file using verb IMHEADER.

---

```

AIPS 1: Image=MULTI (UV) Filename=UV .QSO . 1
AIPS 1: Telescope=GMRT Receiver=GMRT
AIPS 1: Observer= User #= & 501 &
AIPS 1: Observ. date=01-JUN-2012 Map date=19-JUN-2015
AIPS 1: # visibilities 746460 Sort order TB
AIPS 1: Rand axes: UU-L-SIN VV-L-SIN WW-L-SIN SUBARRAY TIME1
AIPS 1: SOURCE FREQSEL ANTENNA1 ANTENNA2
AIPS 1: -----
AIPS 1: Type Pixels Coord value at Pixel Coord incr Rotat
AIPS 1: COMPLEX 3 1.0000000E+00 1.00 1.0000000E+00 0.00
AIPS 1: STOKES 2 -1.0000000E+00 1.00 -1.0000000E+00 0.00
AIPS 1: FREQ 512 1.0376666E+09 0.50 -8.1380205E+03 0.00
AIPS 1: IF 1 1.0000000E+00 1.00 1.0000000E+00 0.00
AIPS 1: RA 1 00 00 00.000 1.00 3600.000 0.00
AIPS 1: DEC 1 00 00 00.000 1.00 3600.000 0.00
AIPS 1: -----
AIPS 1: Coordinate equinox 2000.00
AIPS 1: Maximum version number of extension files of type HI is 1
AIPS 1: Maximum version number of extension files of type AN is 1
AIPS 1: Maximum version number of extension files of type FQ is 1
AIPS 1: Maximum version number of extension files of type SU is 1
AIPS 1: Maximum version number of extension files of type CL is 2
AIPS 1: Maximum version number of extension files of type NX is 1
AIPS 1: Maximum version number of extension files of type FG is 1
AIPS 1: Maximum version number of extension files of type PL is 1
AIPS 1: Maximum version number of extension files of type SN is 2
AIPS 1: Maximum version number of extension files of type BP is 1

```

---

Contents of all the tables can be viewed using task ‘PRTAB’.

```

>task ‘prtab’
>inext ‘su’
>go

```

To delete a table of any extension use the verb EXTDEST.

For example:

```

>inext ‘sn’           extension table type
>invers 0            version number of table to delete
>go extdest

```

Every uv and image file has an associated ‘history’, or HI, file. This HI ‘extension’ of the data set stores important information about the processing done so far on the data in the file. Every AIPS task and verb that alters either the data or the file header will record its key parameters in the history file. The history file is written to tape when you use FITS format, so you can preserve it for reference in later AIPS sessions. In general, each ‘card’ in the history file begins with the task or verb name. It then gives one or

more of the input adverb values it used (i.e. the defaults are filled in). All or parts of the file may be displayed on your terminal or printed on the line printer. For example, use:

```
>indisk n
>getn <catalog number> to select the file to be displayed
>prtask 'UVMAP' to examine only history information from UVMAP
>docrt 1 to direct the display to your terminal, using its full width
>prithi to print the UVMAP history
or
>prtask ' ' to select all history cards and direct the output to the line
printer
>prithi to print the full history file
```

Each time a task is caused to execute (via the verb GO), the adverb values sent to the task are saved in a special Task parameter file. Only one set of values is stored for any given task, but an unlimited number of tasks may have their values stored. The file belongs to the user (by login number) and may be used with any of the interactive AIPS. The input adverb values associated with a task or a verb can be retrieved by the command:

```
> tget name
TGET will therefore recover the last set of input adverbs used to execute the task.
```

Exiting

To exit from AIPS type:

```
> exit to leave TV, message, and graphics servers running, or
> kleenex to kill server processes as well as AIPS
```



## Appendix B

# Getting started with AIPS

### B.1 Starting the AIPS program

Get into the directory where AIPS is installed.

```
$source LOGIN.CSH
```

```
$aips
```

This will begin AIPS.

You will be told about the assigned printer queue, data disks, and tape devices. If all is going well it will then tell you:

```
I am guessing you are at a workstation called localhost
```

```
Starting local TV servers on localhost
```

where *localhost* is the name of your workstation.

Notice the line above that says “Starting local TV servers on localhost”. At that point, the process of figuring out what computer you’re running on and what display you’re sitting at (they may be different) is shed in an asynchronous way while the main process of starting the AIPS program proceeds.

Any news messages about your AIPS installation will then appear. Finally, you should see the messages:

```
Starting up 31DEC15 AIPS with normal priority
```

Few more messages will appear in the same window, where each of the first four messages should announce the starting of one of the servers.

```
XASERVERS: Start TV LOCK daemon TVSERV on localhost
```

```
XASERVERS: Start XAS on localhost, DISPLAY localhost:0
```

```
XASERVERS: Start graphics server TEKSRV on localhost, DISPLAY localhost:0
```

```
XASERVERS: Start message server MSGSRV on localhost, DISPLAY localhost:0
```

```
XAS: ** TrueColor FOUND!!!
XAS: *** Using shared memory option for speed ***
TVSERVER: Starting AIPS TV locking, Inet domain
BEGIN THE ONE TRUE AIPS NUMBER n (release of 31DEC15) at priority 0
```

where 31DEC15 identifies the release of AIPS and  $n$  is a number between 1 and 6 (typically). If this is the only AIPS session on the computer, you should be assigned  $n = 1$ , with higher numbers used for additional sessions. If you start with  $n > 1$ , someone else may be using your computer remotely. AIPS will then tell which TV and graphics devices have been assigned to you:

```
AIPS n: You are assigned TV device nn
AIPS n: You are assigned graphics device mm
where nn and mm are numbers assigned to your workstation.
```

The TEK server (TEKSRV) will appear in iconified form somewhere on the screen, while the message server (MSGSRV) and the XAS TV server (AIPS TV) appears in opened form.

If the TV does not start, use

```
$aips tv=local
```

The “TV=local” option allows use of Unix based sockets for the TV and other servers.

AIPS will now ask you for your user number and provide a ? prompt:

```
AIPS n: Enter user ID number
```

```
?uuuu
```

where *uuuu* is the number assigned to you for the local AIPS system (in decimal form). User Id should be greater than 100.

For example enter:

```
?101
```

The AIPS prompt

```
>
```

should now appear.

## Appendix C

# Step by Step manual for Absorption line Spectroscopy

Before starting AIPS, create an environment variable pointing at the disk directory containing the data files.

```
$ cd < data area >
```

followed by

```
$ setenv MYDATA 'pwd'
```

if you use C-shell or its variants or

```
$ export MYDATA='pwd'
```

if you use the bash shell.

where pwd is the complete path of the data area.

*Remark 1.* Note the back tick marks surrounding the pwd.

Then start AIPS.

If you do not want to create an environment variable, then specify the data area path while loading the data into AIPS as shown below.

### C.1 Loading the data

- The FITS file are loaded using task 'FITLD'. This FITS file is a multi-source file, containing observations for all your sources: flux calibrators, phase calibrators, and target sources.

```
>task 'fitld'
```

```
>datain 'MYDATA:QSO.FITS' if the environment variable is created
```

or

```
>datain '/lhome/guest/DATA/LOCALHOST_1/QSO.FITS'
                                     if the environment variable is not created
>outname 'UV'                        specifies 'name' field for the output data file
>outclass 'QSO'                      specifies 'class' field for the output data file
>inp
>go
```

where QSO.FITS is the name of the fits data file to be loaded and /lhome/guest/-DATA/LOCALHOST\_1/ is its complete path.

*Remark 2.* Note the incomplete quote in datain command.

UV.QSO.1 will be created in User's UV catalog 1 on the specified disk drive.

Keep an eye on the MSGSRV while running any task to ensure that no errors have occurred and the task have been completed successfully.

- The UV data loaded into AIPS is required to be indexed for the speedy access of the data set. Index the UV data using task 'INDXR'.

```
>task 'indxr'
>getn 1                               to get the file on catalog 1
>infile ' '
>go
```

The verb INFILE is used to specify the name of some disk file outside the usual AIPS catalog system to be used as input to an AIPS verb or task, null value ' ' means no subsidiary file. Task 'INDXR' will create NX table and a null calibration table CL version number 1.

- The list of sources and calibrators observed can be checked using task 'LISTR'.

```
>task 'listr'
>optype 'scan'                       to select scan summary listing
>doctr 1                             to direct the display to your terminal, using
                                     its full width
>go
```

A part of 'LISTR' output which will appear on the terminal is shown below.

---

```

Source summary
Velocity type = 'TOPOCENT'      Definition = 'RADIO'

ID Source           Qual  Calcode  RA(2000.0)      Dec(2000.0)  No. vis
1 3C286             : 0000           13:31:08.2856   30:30:32.863  35670
2 1445+099         : 0001    C     14:45:16.4759   09:58:36.070  120495
3 J1443+0214       : 0000           14:43:04.5061   02:14:19.270  556800
4 3C468.1          : 0000           23:50:54.8774   64:40:18.337  33495

ID      Source      Freq(GHz)  Velocity(Km/s)  Rest freq (GHz)
1      All Sources      1.0377      0.0000          0.0000

Frequency Table summary
FQID IF\#      Freq(GHz)  BW(kHz)  Ch.Sep(kHz)  Sideband  Bandcode
1      1          1.03766662  4166.6665  -8.1380      1

```

---

If you want to print the output of task 'LISTR' on the line printer then use,

```
>docrt -1
>outprint ' '
```

To make a text file instead, use

```
>docrt -1
>outprint '/lhome/guest/DATA/LOCALHOST_1/listr.txt'
```

Keep the output for future reference. Note that the frequency in the header of a multi-source file is always the sky frequency in the center of the band of the first scan of the observation.

## C.2 Flagging and Editing

- Editing of data set is done to remove the poor quality data from further analysis. For this purpose it is required to display the data set in various ways to identify bad data.

Task 'VPLOT' can be used to plot  $u, v$  database making a plot file or can be viewed on AIPSTV as plot of amplitude and timerange, phase and timerange, etc. for each baseline and each channel. First we look at all the baselines for all channels to decide a reference 'good channel', as the flagging is needed to be done to the whole data set with this good channel as the reference. Inspect each source, Stokes, and IF separately.

```

>task 'vplot'
>getn 1           to get the file on catalog 1
>sour ' '        ' ' indicates all sources on the multi-source file 1
>stokes 'rr' / 'll' specifies stokes type to be plotted
>bchan 1         start channel
>echan 0         end channel
>ante 0          antennas to be plotted, 0 indicates all antennas
>base 0          baselines between antennas named in ANTENNAS
                  and those named in BASELINE are selected, 0
                  indicates all baselines
>timerang 0     specifies timerange, 0 indicates for all timerange
>nplots 6       maximum number of plots per page
>dotv 1         plot directly on the TV device
>inp
>go

```

Thus 6 plots will appear at a time on AIPSTV. AIPSTV functions refer to 'buttons' A, B, C, and D for the purpose of signalling conditions to the software which will appear on the MSGRV.

For example: Press A on AIPSTV - to pause indefinitely.

- From the plots, specially of the reference channel, bad data can be identified for primary flagging. The exact timerange for which data is bad can be found by zooming into that particular baseline using verb TVINIT (tvin).

```

>tvin
>tget vplot
>ante 1
>base 17
>timerang 01 14 41 40 01 15 05 00
>go

```

where 01 14 41 40 01 15 05 00 indicates the start day, start hour, start minute, start second, stop day, stop hour, stop minute, stop second respectively.

- Once you have determined which data points to flag, flag them with task 'UVFLG'. You can flag by time-range, baseline, or antenna and you can flag any or all of the Stokes parameters or IFs. To assist in undoing flags, set a REASON. If many flagging criteria are to be supplied at once, then they can be listed in

a '.flg' flag file written in the syntax understandable to AIPS. This '.flg' flag file should be created in a directory whose path can be given while specifying the adverb INTEXT for task 'UVFLG'.

Example for format of '.flg' file:

```
stokes='RR' ante=10,26,27,29 reason='bad-antenna' /
stokes=' ' ante=17 timerange=01,14,41,40,01,15,05,00 reason='bad-timerange' /
stokes='RR' ante=17,19 baselin=24 reason='bad-baseline' /
```

where ante=17,19 baselin=24 indicates that baselines 17-24, 19-24 are to be flagged for all timerange.

- This flag file is then read by task 'UVFLG' used for flagging the data. Using task 'UVFLG' data can be flagged or unflagged by modifying a flag (FG) table.

```
>task 'uvflg'
>intext '/lhome/guest/DATA/LOCALHOST_1/J1443p0214.flg'
>inp
>go
```

The adverb INTEXT specifies the name of the text file containing flagging instructions. If INTEXT is used, then adverbs such as TIMERANGE, BIF, etc. are ignored.

*Remark C.1.* Again note the incomplete quote in intext command.

A flag table (FG) version 1 is created by task 'UVFLG' which is used further by some tasks to edit data.

- The flagged data can be unflagged by specifying the adverb OPCODE as opcode='UFLG' in the same '.flg' file.

For example:

```
stokes='RR' ante=10,26,27,29 opcode='UFLG' reason='bad-antenna' /
```

## C.3 Calibration

### C.3.1 Gain Calibration

The aim of calibration is to determine the complex antenna based gains,  $g_i(t)s$ .

- The true visibility for the flux calibrator say  $V_{act}^{fc}$  is already known and well modelled. Task ‘SETJY’ enters flux calibrator source information  $V_{act}^{fc}$  into the source table (SU).

```

>task ‘setjy’
>sources ‘3C286’ ‘ ’      list of sources
>optype ‘calc’          use the standard Perley-Butler or Baars et al
                        formulae and frequency information in the header
                        to determine the flux densities of the primary
                        calibrator 3C286

>go

```

- The calibration can be done by standard calibration procedures using task ‘CALIB’ for the flux calibrator and phase calibrator separately. If observed visibility for the flux calibrator is say  $V_{ij(obs)}^{fc}$ , then the gain factor can be determined from the equation as,

$$G_{ij}^1 = \frac{V_{ij(obs)}^{fc}}{V_{act}^{fc}} \quad (C.1)$$

Firstly, in the task ‘CALIB’, the calibrating source (calsour) is taken to be flux calibrator. The solutions  $G_{ij}^1$  are determined and stored in solution table SN version 1. Then the phase calibrator is calibrated and solutions  $G_{ij}^2$  are determined at an interval (SOLINT) of 2 minute or less depending on their flux density and written in solution table SN version 2. At this stage the actual flux of the phase calibrator is not known, so AIPS assumes the calibrator to be of 1 Jy.

Let the observed visibility for the phase calibrator be  $V_{ij(obs)}^{pc}$ , then

$$G_{ij}^2 = \frac{V_{ij(obs)}^{pc}}{1Jy} \quad (C.2)$$

```

>task ‘calib’
>calsour ‘3C286’ ‘ ’      to specify a list of calibrators to be included
                        in or excluded from an operation, 3C286 is the
                        flux calibrator source

>bchan 1
>echan 0
>uvran 0 50              specifies minimum and maximum projected
                        baselines to include

>refant 16              specifies the desired reference antenna for

```



antenna based phase like calibration  
**>solint 2** specifies the time interval to use in determining calibration parameters in units of minutes  
**>soltype ‘ ’** specifies the least squares solution type to be used in calibration routines, ‘ ’ indicates normal least squares  
**>inp**  
**>go**

The task ‘CALIB’ for flux calibrator will create solution table SN version 1. REFANT defines the antenna to be used as the reference in the least squares solution. Choose an antenna with good signal to noise and that was present for as long as possible through the observing run.

**>task ‘calib’**  
**>calsour ‘1445+099’ ‘ ’** 1445+099 is the phase calibrator  
**>bchan 1**  
**>echan 0**  
**>uvran 0 50**  
**>refant 16**  
**>solint 2**  
**>soltype ‘ ’**  
**>inp**  
**>go**

The task ‘CALIB’ for phase calibrator will create solution table SN version 2. Less than 2% fraction of solutions outside 2.5 rms value is good and less than 4% outside is acceptable.

While running the task ‘CALIB’, the robustness is used to determine the solutions. This is done by keeping the soltype as ‘ ’. What it essentially does is, recomputes the solutions if the visibility computed for the model differs from the actual measured visibility by certain amount. This can be explained mathematically from equation,

$$\begin{aligned}
 V_{ij(obs)}^{pc}(t) &= G_{ij}(t)V_{ij(act)}^{pc}(t) \\
 &= g_i(t)g_j^*(t)V_{ij(act)}^{pc}(t).
 \end{aligned}
 \tag{C.3}$$

The algorithm tries to minimise the quantity,

$$\sum_{i,j} \frac{(V_{ij(obs)}^{pc}(t) - g_i^{model}(t)g_j^{model}(t)V_{ij(act)}^{pc}(t))^2}{\sigma_{i,j}^2}
 \tag{C.4}$$

iteratively. That is, it determines some  $g_{i,j}^{model}(t)$  and minimises the above quantity. Then recomputes the  $g_{i,j}^{model}(t)$ s and returns for the next iteration. The robustness makes sure that the gains are recalculated if the quantity,  $(V_{ij(ops)}^{pc}(t) - g_i^{model}(t)g_j^{model}(t)V_{ij(act)}^{pc}(t))$  differs by certain defined amount.

- The task ‘GETJY’ determines the flux density of phase calibrator  $V_{act}^{pc}$ , from solution table SN version 1, enter it into the SU table and correct the gains  $G_{ij}^2$  in the SN version 2 table.

$$V_{act}^{pc} = \frac{V_{ij(ops)}^{pc}}{G_{ij}^1}. \quad (C.5)$$

Therefore,

$$G_{ij}^2 = \frac{V_{act}^{pc}}{V_{ij(ops)}^{pc}}. \quad (C.6)$$

Hence, the flux calibrator is taken as the CALSOUR and the phase calibrator is the SOURCE to be calibrated.

```

>task ‘getjy’
>sources ‘1445+099’ ‘ ’ list of sources whose flux densities are to be
                           determined
>calsour ‘3C286’ ‘ ’ list of calibrators to use to determine source
                           flux densities
>snver 0 to write in selected SN table, 0 indicates to
                           write in highest SN version table
>go

```

- Once the gain solutions are determined during the observation scans on the phase calibrators with necessary solution interval, they can be interpolated in time between the calibrator scans, i.e. on the target source. This is done by the task ‘CLCAL’ in AIPS.

```

>task ‘clcal’
>sources ‘ ’
>calsour ‘3C286’ ‘1445+099’ ‘ ’ list of calibrators to use for updating the
                           CL table
>opcode ‘cali’ to merge and smooth SN tables
>snver 0 to write output in highest SN version table
>inver 0 to use highest SN table version
>gainver 1 specifies the input version of the CL table

```

>**gainuse 2** to which the SN tables will be applied  
specifies version number of the output  
CL table

>**refant 16**

>**go**

This task will merge the SN tables and apply them to CL table 1, and write CL table 2.

### C.3.2 Bandpass Calibration

- As the gains are in principle functions of frequency as well, the Bandpass essentially determines the response of the interferometer across the frequency band and hence determines the  $G_{ij}(\nu)$  for all the channels. The bandpass calibration is done by the task ‘BPASS’.

>**task ‘bpass’**

>**calsour ‘3C286’ ‘ ’** list of sources for which bandpass response  
functions are to be determined

>**docal -1** false ( $\leq 0$ ) means do not apply calibration

>**doband -1** false ( $\leq 0$ ) means do not apply bandpass  
calibration

>**solint 0** scan average for multi source data

>**refant 16**

>**bpassprm 0**

>**ichansel 17 17 1 0** array of start, stop, and increment channel  
numbers plus an IF used for channel selection  
in the averaging to compute a channel 0

>**go**

First, bandpass is done for entire time range on the phase calibrator, and the bandpass table BP version 1 is generated which will contain the bandpass response functions of the antenna. Thus, the frequency based gains are determined. The bandpass is run again, but this time for each scan average and applying the previous bandpass table, i.e. applying the gains. Ideally, in this situation the new bandpass table must have gains of the order of unity and phase zero. This should also remain stable in time.

- Task ‘SPLIT’ is used to take out only the target source data from the multi-source data. Also the data from the first and last ten channels are non-trustworthy which can be excluded.

>task 'split'	
>sour 'J1443+0214'	specifies the source list
>stokes ' '	the desired Stokes type of the output data
>docal 1	true (> 0) means apply the selected gain table before the specified operation on the uv data
>doband 3	true then correct the data for the shape of the antenna bandpasses using the BP table specified by bpver, doband 3 indicates that the table entries are interpolated in time using solution weights and the data are then corrected
>gainuse 0	specifies version number of the CL table to apply to multisource files, 0 indicates highest numbered table
>bpver 0	specifies the version of the BP table to be applied if doband > 0 , 0 indicates highest numbered table
>flagver 0	specifies the version of flagging table to be applied, 0 indicates highest numbered table
>bchan 11	first channel to copy
>echan 502	highest channel to copy
>douvcomp -1	false (< 0) implies that do not write the output data in compressed format
>ichansel 0	0 indicates bchan, echan, 1, 0
>go	

The calibrated and flagged target source will be stored in a '.split' file. The adverb docal 1 also tells AIPS tasks to apply the amplitude calibration to the data weights as well as to apply the amplitude and phase calibration to the visibilities.

- The bandwidth smearing is taken care of by averaging the number of channels such that the condition below is satisfied.

$$\frac{\Delta\nu^{reqd}}{\nu_0} \sim \frac{2\theta_{synth}}{\theta_{pri}}. \quad (C.7)$$

where,  $\Delta\nu^{reqd} \rightarrow$  required bandwidth,

$\theta_{synth} \rightarrow$  angle of synthesized beam,

$\theta_{pri} \rightarrow$  angle of primary beam.

This is done by using the task 'SPLAT' on the .split file to collapse the line free channels together which is specified using the adverb ICHANSEL. In case of



> <b>uvran 0 90</b>	(minimum,maximum) projected baselines to include in map, units are kilo lambda
> <b>niter 1000</b>	specifies the clean iteration limit
> <b>nchav 190</b>	number of channels to be averaged together in the gridding process
> <b>dotv 1</b>	to display residuals on TV channel 1
> <b>go</b>	

The parameters `CELLSIZE` and `IMSIZE` used in AIPS are chosen depending on the achievable resolution and the interested size of the field to be imaged. Typically, the `CELLSIZE` is given in arcsec, which is about half the size of the synthesised beam. `IMSIZE` is given in number of pixels which is determined by the size of field one wants to measure.

`UVTAPER` is used while imaging to control the shape of the beam and to weight the sparsely filled UV plane. This parameter in AIPS is set by looking at the UV coverage upto the point where the coverage is more or less uniform.

Once the first image is decent enough, its time to do self calibration.

### C.3.3 Self Calibration

So far all the calibration that were done, was on the primary or the secondary calibrators. To calibrate the target source we relied on the interpolation (in time) of the solutions on the secondary calibrators. Good instrumentation assures that the amplitude variation is stable and slow with time. But, due to ionospheric effects, the phase changes considerably faster. We observe the target source, typically of the order of 20-30 minutes. During this time, the ionosphere changes the phase quite a lot and interpolation of phases from the adjacent scans on the phase calibrator are not adequate. To take care of this variation we perform another calibration for phase, called the self calibration. From the Equation 2.56, determination of phases and amplitude is possible because we know the true visibility of the calibrators for all baselines. After imaging of the target source is done, we considerably know the model of the source and therefore a calibration using the target source itself is possible. The model information of the sources in each facet is contained in the CC table. But, all the components in the table may not be the right representation of the sources. So, we select very strong point sources from the CC table to be used for self calibration. Choosing only strong points may not be the exact model of the sources in the field of interest, but for better estimation of the phases giving a model in which the components has about half the flux as contained in the entire field is good enough.

- Use the task ‘CCMRG’ on the clean image file (.ICL001) to create a new clean components CC table with flux for every pixel merged together. ‘CCMRG’ sorts the contents of a given AIPS clean components table to bring all components with the same position together. It then sums such components and resorts the table into descending order by component flux.

>task ‘ccmrg’

>getn 7 to get the clean image file from catalog slot 7

>go

- Use the task ‘PRTCC’ to print the CC table on the terminal. It gives a running total of the flux and tells the number of first negative component.

>task ‘prtcc’

>doctr 1

>go

- After the correct components are chosen the task ‘CALIB’ is run using the selected model to do self calibration.

>task ‘calib’

>getn 3 to get the .splat file from catalog slot 3

>get2n 7 to get the clean image file from catalog slot 7

>calsour ‘ ’ lists of the calibrator sources for which calibration constants are to be determined

>docal -1

>doband -1

>bpver 0

>ncomp 13 number of non-negative clean components to be used for the model, one value per field (13 in this case, which will change in each round of self calibration)

>refant 16

>solint 2

>snver 1

>solmode ‘P’ specifies the solution mode, ‘P’ indicates phase only

>go

A new SN table will be created.

While running ‘CALIB’ `docal -1` is used so that each new SN table created is independent of entries in last SN table.

- Use task ‘IMAGR’ to see the image after self calibration.

```

>task 'imagr'
>getn 3                               to get the .splat file from catalog slot 3
>sour 'J1443+0214' ' '
>bchan 11
>echan 200
>docal 1
>doband -1
>cellsize 0.8 0.8
>imsize 128 128
>uvtaper 60 60
>uvran 0 90
>niter 1000
>nchav 190
>dotv 1
>go

```

After this step go back to task ‘CCMRG’ and repeat the steps upto ‘IMAGR’ two to three times i.e. run the phase only self calibration loop two to three times. Then finally run the last loop with `solmode ‘A&P’` for amplitude and phase calibration together. This is done to take care of any small variation of amplitude (i.e. instrumental gain).

## C.4 Obtaining the spectrum

- The model image has been obtained using an extra round of calibration as compared to what has been applied to the multi-channel target source data. We need to apply the same calibration to both sets for which use task ‘TACOP’. The task ‘TACOP’ copies AIPS extension files, principally those of table type. The specified output file should not exist before the execution of ‘TACOP’. Use task ‘TACOP’ to copy latest version of `.splat` to `.split` file.

```

>task 'tacop'
>getn 3                               to get the .splat from catalog slot 3

```



<b>&gt;inext 'sn'</b>	extension table type
<b>&gt;invers 0</b>	version number of table to copy
<b>&gt;outname 'J1443+0214'</b>	output image name
<b>&gt;outclass 'split'</b>	output image class
<b>&gt;outseq 0</b>	specifies 'sequence number' field for the output data file, 0 indicates highest sequence number
<b>&gt;outvers 0</b>	specifies the version number to be used on output for an extension file
<b>&gt;inp</b>	
<b>&gt;go</b>	

- Run the task SPLIT once more on the .split file with >docal 1, so that the SN table gets applied.

<b>&gt;task 'split'</b>	
<b>&gt;getn 2</b>	to get the .split file from catalog slot 20
<b>&gt;docal 1</b>	
<b>&gt;doband -1</b>	
<b>&gt;bpver 0</b>	
<b>&gt;flagver 0</b>	
<b>&gt;bchan 11</b>	
<b>&gt;echan 502</b>	
<b>&gt;nchav 0</b>	
<b>&gt;ichansel 0</b>	
<b>&gt;douvcomp -1</b>	false (< 0) implies do not compress the output file
<b>&gt;go</b>	

- Each frequency channel in the spectral-line data set is imaged using the same procedures as would be applied to the single channel in a continuum data set. The channels can be used individually, but usually are assembled into a single data structure with three axes - right ascension, declination, and frequency which is called a data cube. Cubes are convenient for storing, displaying, and manipulating the spectral data.

Now use task 'IMAGR' on the split file created above to generate a spectral data cube.

<b>&gt;task 'imagr'</b>	
<b>&gt;getn 17</b>	to get .split file version 2 from catalog slot 17
<b>&gt;sour 'J1443+0214' ' '</b>	

**>in2name ' '** specifies 'name' field for the 2nd of the input data files used by the task  
**>in2class ' '** specifies 'class' field for the 2nd of the input data files used by the task  
**>in2seq 0** specifies 'sequence number' field for the 2nd of the input data files used by the task  
**>bchan 1**  
**>echan 0**  
**>niter 0**  
**>cellsize 0.8 0.8**  
**>imsize 128 128**  
**>uvtaper 60 60**  
**>uvran 0 90**  
**>docalib -1**  
**>doband -1**  
**>dotv -1**  
**>go**

- Now we need to find BLC (Bottom Left Corner) and TRC (Top Right Corner) to give them as input in task 'ISPEC' so as to get the spectrum of the source from the final clean image. BLC and TRC represent the location of the cell with the highest flux density in the image in which the first two values gives column number and row number of the cell.

**>getn 19** to get the final clean image file from catalog slot 19  
**>tval**  
**>tvwindow**

TVALL is a procedure which combines the separate functions of several verbs. It clears the screen, loads the image into and or more TV channels, etc. The verb goes into an interactive mode at this point and shows some messages in the terminal as:

**AIPS 1: Hit button A to enhance B/W or color alternately**  
**AIPS 1: Hit button B to increment zoom& set zoom center**  
**AIPS 1: Hit button C to decrement zoom & set zoom center**  
**AIPS 1: Hit button D to exit**  
**AIPS 1: Cursor X controls intercept**  
**AIPS 1: Cursor Y controls slope**

To find BLC (bottom left corner) and TRC (Top right corner) interactively use TVWINDOW which will again show messages as:

**AIPS 1: Set B.L.C. : button A, B, or C to change to T.R.C.**

**AIPS 1: Button D to kill and exit**

**AIPS 1: Set T.R.C. : button A or B to repeat B.L.C.**

**AIPS 1: Button C or D to exit**

Now select the bottom left corner and then the top right corner to make a square around the image of the source and as soon as you exit from TVWINDOW, the BLC and TRC will appear in the terminal as:

**AIPS 1: BLC = 58.00 61.00 1.00 1.00 1.00 1.00 1.00**

**AIPS 1: TRC = 68.00 69.00 1.00 1.00 1.00 1.00 1.00**

- Run the task 'ISPEC' to get the first glimpse of the spectrum. Task 'ISPEC' is used to plot and print the average brightness or flux of an area in the first two axes of an image as a function of location on the third axis of an image.

**>task 'ispec'**

**>getn 25** gets spectral data cube J1443+0214.IIM001.2

**>optype 'flux'** plot and print the sum of the valid intensities in the subarray, converted to Jy from Jy/beam in clean images

**>dotv 1**

**>blc 58 61 1 1**

**>trc 68 69 1 1**

**>go**

- The spectral data file containing frequency and flux values for above spectrum can be created outside AIPS catalog system by specifying the adverb OUTPRINT. OUTPRINT is the disk file name in which to save the line printer output.

**>tget ispec**

**>inp**

**>getn 25** gets spectral data cube J1443+0214.IIM001.2

**>dotv -1** false (-1) indicates do not display on TV

**>blc 58 61 1 1**

**>trc 68 69 1 1**

**>outprint '/lhome/guest/DATA/LOCALHOST\_1/spectrum.txt**

**>go**